Monthly Notices
of the
ROYAL ASTRONOMICAL SOCIETY

MNRAS **439,** 3189–3212 (2014)
Advance Access publication 2014 February 26

doi:10.1093/mnras/stt2470

Environmental dependence of bulge-dominated galaxy sizes in hierarchical models of galaxy formation. Comparison with the local Universe

Francesco Shankar,[1⋆] Simona Mei,[1,2] Marc Huertas-Company,[1,2] Jorge Moreno,[3] Fabio Fontanot,[4,5] Pierluigi Monaco,[6,7] Mariangela Bernardi,[8] Andrea Cattaneo,[9] Ravi Sheth,[10,8] Rossella Licitra,[1,2] Lauriane Delaye[1] and Anand Raichoor[1]

[1]*GEPI, Observatoire de Paris, CNRS, Univ. Paris Diderot, 5 Place Jules Janssen, F-92195 Meudon, France*
[2]*University Denis Diderot, 4 Rue Thomas Mann, F-75205 Paris, France*
[3]*Department of Physics and Astronomy, University of Victoria, Victoria, BC V8P 1A1, Canada*
[4]*Heidelberger Institut für Theoretische Studien (HITS), Schloss-Wolfsbrunnenweg 35, D-69118 Heidelberg, Germany*
[5]*Institut für Theoretische Physik, Philosophenweg 16, D-69120 Heidelberg, Germany*
[6]*Dipartimento di Fisica – Sezione di Astronomia, Università di Trieste, via Tiepolo 11, I-34131 Trieste, Italy*
[7]*I.N.A.F, Osservatorio di Trieste, Via Tiepolo 11, I-34131 Trieste, Italy*
[8]*Department of Physics and Astronomy, University of Pennsylvania, 209 South 33rd St, Philadelphia, PA 19104, USA*
[9]*Laboratoire d'Astrophysique de Marseille, UMR 6110 CNRS, Univ. d'Aix-Marseille, 38 rue F. Joliot-Curie, F-13388 Marseille cedex 13, France*
[10]*The Abdus Salam International Center for Theoretical Physics, Strada Costiera 11, I-34151 Trieste, Italy*

Accepted 2013 December 18. Received 2013 December 13; in original form 2013 August 9

ABSTRACT

We compare state-of-the-art semi-analytic models of galaxy formation as well as advanced subhalo abundance matching models with a large sample of early-type galaxies from Sloan Digital Sky Survey at $z < 0.3$. We focus our attention on the dependence of median sizes of central galaxies on host halo mass. The data do not show any difference in the structural properties of early-type galaxies with environment, at fixed stellar mass. All hierarchical models considered in this work instead tend to predict a moderate to strong environmental dependence, with the median size increasing by a factor of ∼1.5–3 when moving from low- to high-mass host haloes. At face value the discrepancy with the data is highly significant, especially at the cluster scale, for haloes above $\log M_{\rm halo} \gtrsim 14$. The convolution with (correlated) observational errors reduces some of the tension. Despite the observational uncertainties, the data tend to disfavour hierarchical models characterized by a relevant contribution of disc instabilities to the formation of spheroids, strong gas dissipation in (major) mergers, short dynamical friction time-scales and very short quenching time-scales in infalling satellites. We also discuss a variety of additional related issues, such as the slope and scatter in the local size–stellar mass relation, the fraction of gas in local early-type galaxies and the general predictions on satellite galaxies.

Key words: galaxies: bulges – galaxies: evolution – galaxies: statistics – galaxies: structure – cosmology: theory.

1 INTRODUCTION

Early-type galaxies in the local Universe are observed to follow a rather tight size–stellar mass relation, with an intrinsic scatter of less than a factor of 2 (e.g. Bernardi et al. 2011a,b; Nair, van den Bergh & Abraham 2011). This basic observational feature still represents a challenge for hierarchical models of galaxy formation that form and evolve spheroidal systems out of a sequence of continuous and chaotic minor and major mergers, possibly creating scaling relations similar in slope but more dispersed (e.g. Nipoti, Treu & Bolton 2008; Shankar et al. 2010b, 2013).

On more general grounds, the different location on the size–mass plane of galaxies at their birth (e.g. Shankar & Bernardi 2009; van der Wel et al. 2009; Shankar et al. 2010a; Poggianti et al. 2013), as well as their environment at later times (e.g. Valentinuzzi et al. 2010a), may naturally imprint different evolutionary paths and thus different sizes to galaxies of similar stellar mass, further contributing to enhance the expected final dispersion in scaling relations. In hierarchical models up to 80 per cent of the final stellar mass of

⋆ E-mail: F.Shankar@soton.ac.uk

© 2014 The Authors
Published by Oxford University Press on behalf of the Royal Astronomical Society

Downloaded from http://mnras.oxfordjournals.org/ at INAF Trieste (Osservatorio Astronomico di Trieste) on January 8, 2016

massive bulge-dominated galaxies is predicted to be assembled via a sequence of major and minor mergers (e.g. De Lucia et al. 2006, 2011; Fontanot et al. 2011; Khochfar et al. 2011; Shankar et al. 2013; Wilman et al. 2013). Minor mergers, in particular, have been proposed as a possible driver for the size expansion of the most massive early-type galaxies from compact, red nuggets to the large ellipticals in the local Universe (Naab, Johansson & Ostriker 2009; van Dokkum et al. 2010). Possibly being more frequent in denser environments, mergers are then believed to naturally produce larger galaxies with respect to similarly massive counterparts in the field (e.g. Shankar et al. 2013, and references therein). However, although this conjecture has been put forward in the literature (e.g. Cooper et al. 2012), it still needs to be properly verified in the context of extensive hierarchical galaxy formation models, a task we start exploring in this work.

On the observational side, studies have recently focused on the environmental dependence of the mass–size relation for early-type galaxies, going from the local Universe (e.g. Guo et al. 2009; Weinmann et al. 2009; Maltby et al. 2010; Valentinuzzi et al. 2010a; Huertas-Company et al. 2013a; Poggianti et al. 2013), up to $z \sim 1$–2 (e.g. Valentinuzzi et al. 2010b; Cooper et al. 2012; Mei et al. 2012; Raichoor et al. 2012; Delaye et al. 2013; Huertas-Company et al. 2013a; Strazzullo et al. 2013). In the local Universe several groups tend to confirm the absence of any environmental dependence (e.g. Guo et al. 2009; Weinmann et al. 2009; Huertas-Company et al. 2013a), at least for massive ($M_{\rm star} \gtrsim 10^{11}\,{\rm M}_{\odot}$) early-type galaxies. Some studies find cluster early-type galaxies being slightly smaller than field ones (e.g. Valentinuzzi et al. 2010a; Poggianti et al. 2013). One caveat, however, is that a large fraction of lenticulars is contained in galaxy cluster samples (see, e.g. table 2 in Poggianti et al. 2013). Lenticulars tend to appear more compact at fixed stellar mass (Maltby et al. 2010; Bernardi et al. 2013; Huertas-Company et al. 2013a), thus possibly influencing the analysis of samples with significant contaminations from this latter type of galaxies.

Despite some minor observational issues which still need to be clarified, any size increase with environment (labelled by halo mass) seems to be overall quite negligible in the local Universe, at least for massive early-type galaxies ($M_{\rm star} > 10^{11}\,{\rm M}_{\odot}$). This may pose an interesting observational challenge for hierarchical galaxy evolution models, which would naively predict a stronger galaxy growth in denser environments.

At higher redshifts, there is instead growing evidence for a possibly accelerated structural evolution of massive early-type galaxies in very dense, cluster environments. Preliminary studies (e.g. Rettura et al. 2010; Raichoor et al. 2012) claimed for broadly similar or slightly different optical morphologies for early-type galaxies in the cluster and in the field. Using the larger and more uniform sample of galaxies extracted from the HAWK-I cluster survey at $0.8 < z < 1.5$, Delaye et al. (2013) find instead that early-type galaxies living in clusters are about 50 per cent larger than equally massive counterparts in the field (but see also Newman et al. 2013). Papovich et al. (2012), Bassett et al. (2013), Lani et al. (2013) and Strazzullo et al. (2013) find larger galaxies with respect to the field in (proto) clusters at comparable or even higher redshifts $z \sim 1$–2, and Cooper et al. (2012) at intermediate redshifts $0.4 < z < 1.2$ in DEEP data also claimed larger early-type galaxies in denser environments.

Understanding the degree of redshift evolution of early-type galaxies in different environments is beyond the scope of this work. Here we will mainly focus on model predictions and data at $z = 0$, where the statistics is much higher and at least some of the measurements more secure. We defer the comparison to higher redshift data in separate work (Shankar et al., in preparation). The aim of this paper is to carefully re-analyse the predictions of state-of-the-art hierarchical semi-analytic models (SAMs) and semi-empirical models of galaxy formation with respect to their predictions on bulge sizes, and their dependence on environment (halo mass) in the local Universe. By comparing different models developed under different techniques and physical assumptions, the goal is to discern under which conditions the models can better line up with the data. We note that interesting alternatives or more general interpretations that do not necessarily rely on solely (dry) merging, have been discussed in the literature to evolve early-type galaxy sizes (e.g. Fan et al. 2010; Ragone-Figueroa & Granato 2011; Chiosi, Merlin & Piovan 2012; Carollo et al. 2013; Ishibashi, Fabian & Canning 2013; Kravtsov 2013; Posti et al. 2013; Stringer et al. 2013, and references therein), but we will reserve the investigation of these models for future studies.

The structure of the paper is as follows. We start by briefly introducing the data sets used as a comparison in Section 2. We then proceed by introducing the main features of the reference models adopted in this study in Section 3. Our main results are then presented in Section 4, and further discussed, along with other caveats, in Section 5 and the appendices. We conclude in Section 6.

2 DATA

The early-type galaxy sample used as the reference data in this study is the one collected and studied in Bernardi et al. (2013) and Huertas-Company et al. (2013b), and we refer to those papers for full details on image fitting and morphological classification. We here briefly recall that galaxies are extracted from the Sloan Digital Sky Survey (SDSS) DR7 spectroscopic sample (Abazajian et al. 2009), with an early-type morphology and redshift $0.05 < z < 0.2$ based on the Bayesian automated morphological classifier by Huertas-Company et al. (2011). The latter performed the automated classification of the full SDSS DR7 spectroscopic sample based on support vector machines, and associated with every galaxy a probability to be in four morphological classes (E, S0, Sab and Scd). Early-type galaxies are defined as those systems with a probability PROBE" to be early type (elliptical-E or lenticular-S0) greater than 0.5. We note that the results are not significantly altered if we select galaxies based only on the probability for only ellipticals (PROBELL") or for ellipticals plus lenticulars (PROBELL"+PROBS0"). This is expected, given that central, bulge-dominated galaxies, especially in the range of interest to this work ($M_{\rm star} \gtrsim 2 \times 10^{11}\,{\rm M}_{\odot}$), tend to be dominated by ellipticals.

Halo masses are taken from the group and cluster galaxy catalogue by Yang et al. (2007), updated to the DR7. As in Huertas-Company et al. (2011), we restricted the analysis to groups with $z < 0.09$ (for completeness reasons) and at least two members, and also removed those objects affected by edge effects (fedge < 0.6). This selection ensures that ∼80 per cent of the groups have $\lesssim$20 per cent contamination from interlopers. On the assumption of a one-to-one relation (with no scatter), Yang et al. (2007) assigned halo masses via abundance matching, i.e. via rank ordering between the total galaxy luminosity/stellar and halo mass functions. In the specific, we use as halo mass estimate those based on the characteristic luminosity of the group. The expected uncertainties on such halo masses are ∼0.2–0.3 dex (Yang et al. 2007).

Galaxy sizes are circularized effective radii obtained from the 2D Sérsic fits performed by Bernardi et al. (2012) using the PYMORPH package (Vikram et al. 2010), which can fit seeing convolved two components models to observed surface brightness profiles.

Downloaded from http://mnras.oxfordjournals.org/ at INAF Trieste (Osservatorio Astronomico di Trieste) on January 8, 2016

Stellar masses have been obtained from the MPA-JHU DR7, derived through spectral energy distribution fitting using the Bruzual & Charlot (2003) synthesis population models, and converted to a Chabrier (2003) initial mass function (IMF), in line with the theoretical models described below.

Our team has actively explored the structural properties of early-type galaxies at both low and high redshifts. We here summarize some of our previous empirical results relevant to this work. In Bernardi et al. (2012) we quantified the systematics in the size–luminosity relation of galaxies in the SDSS main sample which arise from fitting different 1- and 2-component model profiles to the images. In particular, we emphasized that despite the half-light radius can vary with respect to different types of fitting, the global net effect on the *R*–*L* relation is small, except for the most luminous tail, where it curves upwards towards larger sizes. Compared to lower mass galaxies and previous work in the local Universe, the slope is in fact $\beta \sim 0.85$ instead of the commonly reported slope of $\beta \sim 0.5$–0.6 (e.g. Shen et al. 2003; Cimatti, Nipoti & Cassata 2012). This difference is mainly due to the way Bernardi et al. (2012) fit the light profile, and in part to the sky subtraction. We will further expand on this point in Section 4.4. In Huertas-Company et al. (2013a) we used the above defined sample of $z \sim 0$ SDSS early-type galaxies to point out a negligible dependence of the sizes on environment, at fixed stellar mass. More specifically, we were able to demonstrate via detailed Monte Carlo simulations that considering our observational errors and the size of the sample, any size ratio larger than 30–40 per cent between massive galaxies ($\log M_{\rm star}/{\rm M}_{\odot} > 11$) living in clusters and in the field could be ruled out at 3σ level. The analysis yielded similar results irrespective of the explicit galaxy selection, either on type (central/satellite), star formation rate, exact early-type morphology, or central density, at least for galaxies above $\gtrsim 10^{11}\,{\rm M}_{\odot}$. In the same work, we also emphasized that our findings on a null dependence on environment were not induced by a galaxy sample biased towards possibly more evolved systems with higher values[1] of the Sérsic index *n*. Our early-type galaxy sample is in fact characterized by broad Sérsic index distributions, with a slight dependence on stellar mass. More quantitatively, one could broadly define a linear relation of the type $n - \log M_{\rm star}$, with a slope of $\sim$0.8 and scatter of $\sim$1.2. We will further discuss the negligible environmental dependence of the size–stellar mass relation in SDSS early-type galaxies in Section 4.5.2. In the following, we will use this large and accurate galaxy sample of early-type galaxies as a base to compare with detailed predictions from a suite of SAMs and semi-empirical models presented in the next section.

3 THEORETICAL MODELS

Before entering into the details of each galaxy formation model adopted in this work, we first summarize some key, common properties of how the mass and structure of bulges are evolved in hierarchical models. Clearly, models include a variety of physical processes, including gas cooling, supernova feedback, stellar/gas stripping, supermassive black hole feeding and feedback, etc. and we defer the reader to the original model papers (cited below) for complete details on their full implementations. In the following, we will mainly focus on those physical processes which have a direct impact on shaping bulge sizes.

Galaxies evolve along dark matter merger trees via in situ star formation and mergers from incoming satellites. Galaxies are usually assumed to initially have a disc morphology via conservation of specific angular momentum, and then evolve their morphology via mergers and disc instabilities. When galaxies become satellites in larger haloes, they are assigned a dynamical friction time-scale $t_{\rm df}$ for final coalescence with the central galaxy

$$t_{\rm df} = t_{\rm dyn} T(M_{\rm halo}/M_{\rm s}, {\rm orbit}), \quad (1)$$

where T is a general function of the mass ratio between main dark matter halo $M_{\rm halo}$ and the satellite $M_{\rm s}$, as well as the orbital parameters. The dynamical time-scale is defined as $t_{\rm dyn} = 0.1 H(z)^{-1}$, where $H(z)$ is the Hubble's parameter. Each model generally adopts a somewhat different analytic treatment for $t_{\rm df}$, which in turn has an impact on the cumulative rate of mergers per galaxy. In the following, we will only briefly emphasize the key differences relevant to our discussion. Full details on the comparison of dynamical friction time-scales among different models can be found in, e.g. De Lucia et al. (2010).

When a merger between a central and a satellite galaxy actually occurs, models broadly distinguish two possibilities. In violent *major* mergers (in which the ratio of the baryonic masses of the progenitors is usually assumed to be $M_2/M_1 > 0.3$), discs are completely destroyed forming a spheroid.[2] The remnant's stellar mass is then composed of the stellar mass of the progenitors and a given fraction, depending on the model, of the gas present in the merging discs, properly converted into stars in a burst. In *minor* mergers ($M_2/M_1 < 0.3$), the stars of the accreted satellite are added to the bulge of the central galaxy, while any accreted gas can be either added to the main gas disc, without changing its specific angular momentum, or converted to stars and added to the bulge, according to the model, as detailed below.

Particularly relevant for the present study is the computation of bulge sizes. We summarize in Table 1 all the key physical parameters adopted in the hierarchical models considered in this work, playing a significant role in shaping the size distribution of bulges and spheroids. A description of the relevant processes and related parameters is given below. For the rest of the paper we will mainly focus our attention on bulge-dominated galaxies with bulge-to-total stellar mass ratio $(B/T) > 0.5$, although we will discuss the effects of tighter cuts in the selection where relevant.

Cole et al. (2000) were the first to include in their model an analytic treatment of bulge sizes, and all the other hierarchical galaxy formation models considered here followed their initial proposal. The size of the remnant $R_{\rm new}$ is computed from the energy

[1] In hierarchical scenarios, for example, more evolved systems, i.e. with more mergers, could be expected to have, on average, higher values of the Sérsic index (e.g. Hopkins et al. 2009).

[2] None of the models considered in this work include disc survival after a major merger, even if the merger is sufficiently gas rich. However, this is believed to be an important aspect only when dealing with the evolution of more disc-dominated, less massive systems, such as lenticulars. Disc survival is believed to play a relatively minor role for the bulge-dominated massive ($\gtrsim 2 \times 10^{11}\,{\rm M}_{\odot}$) galaxies of interest here, with relatively minor gas leftover after the major merger, and late mass assembly dominated by minor, dry mergers. For the latter systems, the half-mass radius is largely dominated by the bulge component, as also empirically confirmed from detailed bulge-to-disc decompositions morphological fitting (Bernardi et al. 2013). Recent semi-analytic modelling (De Lucia et al. 2011; Wilman et al. 2013) confirm disc survival to be a non-negligible component mainly for low to intermediate masses, and at high redshifts. We will anyway discuss disc survival where relevant.

Downloaded from http://mnras.oxfordjournals.org/ at INAF Trieste (Osservatorio Astronomico di Trieste) on January 8, 2016

Table 1. List of the main parameters adopted in the hierarchical galaxy formation models discussed in this work responsible for shaping the sizes of bulges and spheroids.

Parameter	Description	Value
$\mu = M_{\rm sat}/M_{\rm cen}$	Ratio between the baryonic masses of satellite and central. Mass ratios above/below this threshold are treated as major/minor merging.	0.3
$e_{\rm burst}$	Fraction of cold gas converted to stars in a merging and added to the bulge.	0–1
$(t_{\rm df}/t_{\rm dyn})/(t_{\rm df}/t_{\rm dyn})_{\rm num\ sims}$	Ratio of the dynamical friction time-scale in units of the dynamical time adopted in models, compared to that from controlled numerical simulations (see fig. 14 in De Lucia et al. 2010).	0.1–1
$f_{\rm orb}$	Average orbital energy of the merging systems.	0–1
$R_{\rm new}$[dissipation]/$R_{\rm new}$[dissipationless]	Ratio between size of the remnant in the dissipation and dissipationless case.	∼0.1–1
$f_{\rm int}$	Gravitational interaction term between the disc and the bulge.	2
ϵ	Ratio between reference circular velocity and the circular velocity of the disc.	∼1

conservation between the sum of the self-binding energies of the progenitor galaxies, and that of the remnant (Cole et al. 2000)

$$\frac{(M_1+M_2)^2}{R_{\rm new}} = \frac{M_1^2}{R_1} + \frac{M_2^2}{R_2} + \frac{f_{\rm orb}}{c}\frac{M_1 M_2}{R_1+R_2}, \quad (2)$$

where M_i, R_i, are, respectively, the total masses and half-mass radii of the merging galaxies. The form factor c, depends weakly on the galaxy density profile varying from 0.45 for pure spheroids to 0.49 for exponential discs (Cole et al. 2000). The factor $f_{\rm orb}$ instead parameterizes the (average) orbital energy of the merging systems, ranging from zero for parabolic orbits, to unity in the limit in which the two pre-merging galaxies are treated as point masses in a circular orbit with separation $R_1 + R_2$. Effectively, the ratio $f_{\rm orb}/c$ can be considered as a free parameter.

Equation (2) does not include gas dissipation which, as revealed by high-resolution hydrosimulations (e.g. Hopkins et al. 2009; Covington et al. 2011, and references therein), tends to shrink bulges formed out of gas-rich mergers, more than what would be predicted by the dissipationless mergers defined in equation (2). Hopkins et al. (2009) proposed a rather simple prescription to include gas dissipation in mergers as

$$R_{\rm new} = \frac{R_{\rm new}[\rm dissipationless]}{1+F_{\rm gas}/f_0}, \quad (3)$$

where $f_0 = 0.25-0.30$, $F_{\rm gas}$ is the ratio between the total mass of cold gas and the total cold plus stellar mass (inclusive of the mass formed during the burst) of the progenitors, and $R_{\rm new}$[dissipationless] is computed from equation (2). We will discuss the impact of gas dissipation in the relation between size and environment.

In most of the models bulges are also assumed to grow via disc instabilities. The general criterion adopted for disc instability in the SAMs discussed here is expressed as (Efstathiou, Lake & Negroponte 1982)

$$\epsilon > \frac{V_{\rm ref}}{\sqrt{G M_{\rm disc}/R_{\rm disc}}}, \quad (4)$$

with the circular velocity of the disc expressed in terms of its mass $M_{\rm disc}$ and half-mass radius $R_{\rm disc}$ (for exponential profile, equal to $1.68R_{\rm D}$, with $R_{\rm D}$ the disc scalelength). The reference velocity $V_{\rm ref}$ is usually expressed as a linear function of the circular velocity of the host halo or the disc itself, while ϵ is a real number of order unity, as detailed below. When the circular velocity of the disc becomes larger than a given reference circular velocity, then the disc is considered unstable and mass is transferred from the disc to the bulge. Equation (4) expresses the physical condition that when the disc becomes sufficiently massive that its self-gravity is dominant, then it tends to be unstable to any small perturbation.

In the case of disc instabilities the size of the bulge is also computed via an energy conservation equation (Cole et al. 2000) equivalent to equation (2)

$$\frac{(M_{\rm bulge}+M_{\rm disc})^2}{R_{\rm new}} = \frac{M_{\rm bulge}^2}{R_{\rm bulge}} + \frac{c_D}{c_B}\frac{M_{\rm disc}^2}{R_{\rm disc}} + \frac{f_{\rm int}}{c_B}\frac{M_{\rm bulge}M_{\rm disc}}{R_{\rm bulge}+R_{\rm disc}}, \quad (5)$$

which expresses a merger-type condition between the unstable disc with mass $M_{\rm disc}$ and half-mass radius $R_{\rm disc}$, and any pre-existing bulge with mass $M_{\rm bulge}$ and half-mass radius $R_{\rm bulge}$. Following Cole et al. (2000), all models below use the values of $c_B \sim c_D \sim 0.5$, for the bulge and disc form factors, and $f_{\rm int} = 2$ for the constant parameterizing the gravitational interaction term between the disc and the bulge. As discussed by Guo et al. (2011), a higher value of $f_{\rm int} = 2$ for the interaction term with respect to the value of $f_{\rm orb} \lesssim 1$ usually used in equation (2), physically takes into account that the interaction in concentric shells is stronger than in a merger. This in turn implies that for similar stellar mass of the remnant bulge, a disc instability will inevitably produce more compact sizes with respect to a merger. In other words, in this formalism mergers are considered to be more efficient in building larger bulges and spheroids.

3.1 The Durham model by Bower et al. (2006)

One popular rendition of the Durham galaxy formation models[3] is the one by Bower et al. (2006, hereafter B06). This model is built on the Millennium I simulation (Springel 2005), composed of

[3] Available at http://www.g-vo.org/MyMillennium3.

Downloaded from http://mnras.oxfordjournals.org/ at INAF Trieste (Osservatorio Astronomico di Trieste) on January 8, 2016

$N = 2160^3$ dark matter particles of mass $8.6 \times 10^8\, h^{-1}\, \mathrm{M}_\odot$, within a comoving box of size $500\, h^{-1}$ Mpc on a side, from $z = 127$ to the present, with cosmological parameters $\Omega_\mathrm{m} = 0.25$, $\Omega_\mathrm{b} = 0.045$, $h = 0.73$, $\Omega_\Lambda = 0.75$, $n = 1$ and $\sigma_8 = 0.9$.

Galaxies in these models are self-consistently evolved within merger trees which differ with respect to the original ones presented by Springel (2005), both in the criteria for identifying independent haloes, and in the treatment and identification of the descendant haloes (see details in Harker et al. 2006). The dynamical friction time-scales adopted by B06 follow Cole et al. (2000) and, as shown in De Lucia et al. (2010), they can be factors of $\gtrsim$2–3 to $\gtrsim$10, respectively, for major and minor mergers, lower than those extracted from controlled numerical, high-resolution cosmological simulations (e.g. Boylan-Kolchin, Ma & Quataert 2008).

In a major merger, following Cole et al. (2000), B06 assume that a single bulge or elliptical galaxy is produced, and any gas present in the discs of the merging galaxies is converted into stars in a burst. In a minor merger, all the stars of the accreted satellite are added to the bulge of the central galaxy, while the gas is added to the main gas disc. In equation (4) B06 set V_ref as the circular velocity at the half-mass radius of the disc, with $\epsilon \sim 1$, and assume that when the disc goes unstable the entire mass of the disc is transferred to the galaxy bulge, with any gas present assumed to undergo a starburst, and adopt the values of $c_B = 0.45$ and $c_D = 0.49$ for the bulge and disc form factors.

Finally, following Cole et al. (2000), B06 also include some halo adiabatic contraction prescriptions that slightly modify the sizes as calculated out of equations (2) and (5), but the effects of these re-adjustments are relatively small (e.g. González et al. 2009).

3.2 The Munich model by Guo et al. (2011)

One of the latest renditions of the Munich model[4] has been published in Guo et al. (2011, hereafter G11), and we use their run on the Millennium I simulation (with merger trees from Springel 2005). The satellite total infall time is given by the destruction time of the subhalo due to tidal truncation and stripping, plus an additional dynamical friction time-scale down to the coalescence of the subhalo with the centre of the main halo. Overall, the Munich total merging time-scales are comparable to, although in extreme minor merging regime somewhat shorter than, those from high-resolution cosmological simulations (De Lucia et al. 2010).

The G11 model evolves gas and stellar discs in an inside-out fashion, adding material to the outskirts following conservation of angular momentum. G11 have shown that their model is capable of reproducing the size distribution of local discs reasonably well (additional comparisons can be found in, e.g., Fu et al. 2010, 2013; Kauffmann et al. 2012).

As in B06, G11 assume that in minor mergers the pre-existing stars and the gas of the satellite are added to the bulge and to the disc of the primary galaxy, respectively. G11 also allow for some new stars to be formed during any merger following the collisional starburst model by Somerville, Primack & Faber (2001), where only a fraction

$$e_\mathrm{burst} = 0.56 \left(\frac{M_2}{M_1}\right)^{0.7} \qquad (6)$$

of the cold gas of the merging galaxies is converted into stars. The new stars are then added to the bulge or to the disc, depending on the merger begin major or minor, respectively.

When computing bulge sizes, the G11 model also takes into account the fact that only the stellar bulge of the central partakes in a minor merger with the satellite, thus M_1 and R_1 in equation (2) are replaced by the bulge mass and half-mass radius, respectively. In a major merger, G11 limit the virial masses M_1 and M_2 entering equation (2) to the sum of stellar mass plus the fraction of gas converted into stars, assumed to be distributed with an exponential profile with half-mass radius computed following the full prescriptions given in G11. G11 also adopt a fiducial value of $f_\mathrm{orb} = 0.5$ in equation (2).

The disc instabilities are treated somewhat differently in the G11 model. First, in the condition for instability in equation (4), G11 set $\epsilon = 1/\sqrt{3}$ and V_ref equal to the maximum circular velocity of the (sub)halo. Secondly, when a disc goes unstable, only the necessary fraction of stellar mass δM_star in the disc is transferred to the bulge to keep the system marginally stable. Thirdly, G11 adopt equation (5) to compute bulge sizes in disc instabilities *only* if a bulge is already present. If not, then it is assumed that the mass δM_star is transferred, with no loss of angular momentum, from the inner part of the disc (with the exponential-like density profile) to the forming bulge, in a way that the bulge half-mass radius equals the radius of the destabilized region

$$\delta M_\mathrm{star} = 2\pi\Sigma_0 R_\mathrm{D}[R_\mathrm{D} - (R_\mathrm{D} + R_\mathrm{bulge})\exp(-R_\mathrm{bulge}/R_\mathrm{D})], \qquad (7)$$

where R_bulge is the half-mass radius of the newly formed bulge and Σ_0 is the central density of the disc.

3.2.1 *Modifications to the Guo et al. (2011) model*

The G11 model does not include gas dissipation. Shankar et al. (2013) have modified the G11 numerical code to include gas dissipation during *major* mergers as given in equation (3). They also adopted $f_\mathrm{orb} = 0$ together with dissipation, as this combination yielded an improved match to the local size–stellar mass relation. We will discuss the impact of this variant of the G11 model to the general predictions on environment, and label this model as S13 in the following.

3.3 The MORGANA model

The MORGANA model uses as an input the dark matter merger trees obtained with the PINOCCHIO algorithm (Monaco, Theuns & Taffoni 2002). This does not give information on halo substructures. In the original version of MORGANA galaxy merging times are computed using the model of Taffoni et al. (2003), which takes into account dynamical friction, mass-loss by tidal stripping, tidal disruption of substructures and tidal shocks. However, the Taffoni et al. (2003) time-scales have been shown to be significantly shorter than those obtained from *N*-body simulation by, e.g. Boylan-Kolchin et al. (2008).

In this work we will use a version of MORGANA presented in De Lucia et al. (2011) and Fontanot et al. (2011). This implements longer dynamical friction time-scales for satellites, consistent with those of De Lucia & Blaizot (2007). In addition, this version of the model does not include the scattering of stars to the diffuse stellar component of the host halo that takes place at galaxy merging (Monaco et al. 2006). This is particularly relevant for this paper as it maximizes the effect of mass growth via mergers, because satellites retain all their mass before final coalescence thus allowing a more efficient size growth in the remnant (cf. equation 2).

[4] Available at http://www.g-vo.org/MyMillennium3.

Downloaded from http://mnras.oxfordjournals.org/ at INAF Trieste (Osservatorio Astronomico di Trieste) on January 8, 2016

Mergers and disc instabilities move mass from the disc to the bulge component through very similar analytic prescriptions as the ones in B06. In minor mergers ($M_2/M_1 < 0.3$), the whole satellite is added to the bulge, while the disc remains unaffected. The latter characteristic boosts the growth in mass of the centrals, rendering minor mergers more efficient in size growth than for, e.g. the G11 model. In major mergers, all the gas and stars of the two merging galaxies are given to the bulge of the central one. Sizes in mergers follow energy conservation given in equation (2), with $f_{\rm orb}/c = 2$. In addition to these processes, cooling and infall from the halo on to a bulge/disc system is assumed to deposit cold gas in the bulge as well, for a fraction equal to the disc surface covered by the bulge. This is done to let feedback from the central black hole respond quickly to cooling without waiting for a merging or disc instability. This process is responsible for a minor part of mass growth of bulges.

For disc instabilities, MORGANA uses a threshold given by equation (4) with $\epsilon = 0.9$, $V_{\rm ref}$ being the disc rotation velocity [computed with a model like Mo, Mao & White (1998) which takes into account the presence of the bulge] at 3.2 scale radii. In disc instability events this model assumes that 50 per cent of the disc mass is transferred to the bulge, and the size of the forming bulge is given by equation (5) with $C_B = C_D = 0.5$. In this respect, the MORGANA model can be considered to be mid-way between the G11 model characterized by relatively weak disc instabilities, and the B06 model with maximal instabilities. To better isolate the impact of disc instabilities on model results, in the following we will also discuss a realization of the MORGANA model with the same identical prescriptions as the one just described but with no disc instabilities.

3.4 Subhalo abundance matching model

We also include in our analysis the results of a subhalo abundance matching model (SHAM). This approach relies on progressively more popular semi-empirical techniques adopted to study a variety of galaxy properties, from colours to structure (e.g. Vale & Ostriker 2004; Shankar et al. 2006; Hopkins et al. 2009, 2010; Leauthaud et al. 2010; Bernardi et al. 2011a,b; Neistein et al. 2011; Watson, Berlind & Zentner 2012; Yang et al. 2012; Moster, Naab & White 2013). Probing galaxy evolution via a semi-empirical model like the one sketched in this section, allows us to restrict the analysis to just a few basic input parameters, i.e. just the ones defining the underlying chosen physical assumptions (e.g. mergers and/or disc instabilities), as all other galaxy properties are fixed from observations.

Our model starts from 20 000 dark matter merger trees randomly extracted from the Millennium simulation, but uniformly,[5] in the range 10^{11} to 10^{15} $\mathrm{M}_\odot\,h^{-1}$. Inspired by the methodologies adopted by Hopkins et al. (2009) and Zavala et al. (2012), a (central) galaxy inside the main progenitor branch of a tree is at each time step initialized in all its basic properties (stellar mass, gas fraction, structure, etc.) via empirical relations until a merger occurs. Central galaxies are assumed to be initially gas-rich discs, and then evolve into a spheroid via a major merger, and/or grow an inner bulge via minor mergers and/or, possibly, disc instabilities. After a major merger occurs, the central galaxy is no longer re-initialized and it remains frozen in all its baryonic components, although we still allow for stellar and gas mass growth via mergers.

SHAM models have the virtue that they do not require full ab initio physical recipes to grow galaxies in dark matter haloes, as in extensive galaxy formation models (SAMs). This in turn allows to bypass the still substantial unknowns in galaxy evolution about, e.g. star formation, cooling and feedback which in turn may drive more sophisticated galaxy formation models to serious mismatches with basic observables such as the stellar mass function (e.g. Henriques et al. 2012; Guo et al. 2013). SHAM models instead use the stellar mass function and other direct observables as *inputs* of the models, allowing us to concentrate on other galaxy properties, such as mergers and the role of environment, making them ideal, complementary tools for studies such as the one undertaken here.

More specifically, we assume that initially central galaxies are discs with an exponential profile following at all times (we here consider the evolution at $z \leq 3$, where the data are best calibrated) the redshift-dependent $M_{\rm star}$–$M_{\rm halo}$ relation defined by Moster et al. (2013) (for a Chabrier IMF) as

$$M_{\rm star} = 2M_{\rm halo}N\left[\left(\frac{M_{\rm halo}}{M_1}\right)^{-\beta} + \left(\frac{M_{\rm halo}}{M_1}\right)^{\alpha}\right]^{-1}, \quad (8)$$

with all the parameters N, M_1, β and α varying with redshift as detailed in Moster et al. (2013). Despite equation (8) being an improvement with respect to previous attempts, as it takes into account measurement errors on the stellar mass functions, the exact correlation between stellar mass and halo mass is still a matter of debate (e.g. Neistein et al. 2011; Yang et al. 2012). Nevertheless, using other types of mappings (Yang et al. 2012) does not qualitatively affect our global discussion which is mainly based on comparisons at *fixed* bin of stellar mass.

Gas fractions are assigned to each central disc galaxy according to its current stellar mass and redshift using the empirical fits by Stewart et al. (2009)

$$f_{\rm gas} = \left(\frac{M_{\rm star}}{4.5\times10^{11}\mathrm{M}_\odot}\right)^{a(z)}, \quad (9)$$

with $a(z) = -0.59(1+z)^{0.45}$. Disc half-mass, or half-light, radii (which we here assume equivalent, i.e. light traces mass) are taken from the analytic fit by Shen et al. (2003)

$$R_{\rm disc} = \frac{R_0}{(1+z)^{0.4}}M_{\rm star}^{k}\left(1+\frac{M_{\rm star}}{3.98\times10^{10}\,\mathrm{M}_\odot}\right)^{p-k}, \quad (10)$$

with $R_0 = 0.1$, $k = 0.14$, $p = 0.39$ [input stellar masses in equation (10), defined for a Chabrier IMF, are corrected following Bernardi et al. (2010) by 0.05 dex to match the IMF used by Shen et al.]. The extra redshift dependence of $(1+z)^{-0.4}$ in equation (10) at fixed stellar mass is adapted from, e.g. Somerville et al. (2001) and Hopkins et al. (2009). Although observations may provide slightly different normalizations and/or slope for equation (10) (see, e.g. discussion in Bernardi et al. 2012), this does not alter our conclusions.

After a merger we assume the mass assembly and structural growth criteria as in G11. In a major merger the central galaxy is converted into an elliptical, with its stellar mass equal to the sum of those of the merging progenitors as well as the gas converted into stars during the starburst following equation (6). In a minor merger only the stars of the satellite are accreted to the bulge. Bulge sizes are determined from equation (2).

[5] When computing statistical distributions of any quantity extracted from the SHAM model, we will always include proper galaxy weights. The latter are given by computing the ratio between the integral of the halo mass function over the volume of the Millennium simulation and over the bin of halo mass considered, divided by the number of galaxy hosts in the Monte Carlo catalogue in the same bin. We note that even ignoring the weighting would have a negligible impact on any result on the size distributions at fixed stellar mass.

Downloaded from http://mnras.oxfordjournals.org/ at INAF Trieste (Osservatorio Astronomico di Trieste) on January 8, 2016

To each infalling satellite, we assign all the properties of a central galaxy living in a typical halo, randomly extracted from the overall Monte Carlo catalogue of central galaxies, with the same (unstriped) mass as the satellite host dark matter halo at infalling time. Observational uncertainties in calibrating the exact morphologies of especially lower mass galaxies (e.g. Bakos & Trujillo 2012) anyway still limit our true knowledge of merging progenitors, and recent studies seem to show that the vast majority of the high-redshift massive galaxies are disc dominated (e.g. Huertas-Company et al. 2013a, and references therein). By simply approximating all infalling satellites as discs (i.e. with negligible bulges), in line with what assumed by Zavala et al. (2012), any dependence of size with host halo mass would be less strong than the ones actually presented below.

Dynamical friction time-scales are taken from the recent work of McCavana et al. (2012)

$$t_{\rm df} = t_{\rm dyn} \frac{A(M_{\rm halo}/M_{\rm s})^{B}}{\ln(1+M_{\rm halo}/M_{\rm s})} \exp\left[C\frac{J}{J_c(E)}\right]\left[\frac{r_c(E)}{R_{\rm vir}}\right]^{D}, \quad (11)$$

with $A = 0.9$, $B = 1.0$, $C = 0.6$ and $D = 0.1$, but we checked that using the values of these parameters inferred by Boylan-Kolchin et al. (2008) instead yields similar results. Following Khochfar & Burkert (2006), to each infalling satellite we assign a circularity $\xi = J/J_c(E)$ randomly extracted from a Gaussian with average 0.50 and dispersion of 0.23 dex, from which we compute $r_c = R_{\rm vir}\xi^{2.17}/(1-\epsilon)$, with $\epsilon = \sqrt{1-\xi^2}$.

What is also relevant to size evolution of central galaxies, as further detailed below, is how we treat satellite evolution in stellar mass and size once they fall in more massive haloes, i.e. the degree of (gas and star) stripping and/or the amount of residual star formation (which self-consistently grows stellar mass and disc radius). In our basic model, we assume in line with many observational and/or semi-empirical results (e.g. Muzzin et al. 2012; Krause et al. 2013; Mendel et al. 2013; Wetzel et al. 2013; Woo et al. 2013; Yang et al. 2013) that satellite galaxies continue forming stars according to their specific star formation rate (SSFR) for up to a few Gyr. The latter is in agreement with the recent results of Mok et al. (2013), who find any delay between accretion and the onset of truncation of star formation to be $\lesssim$2 Gyr, at least for massive satellites in the range 10^{10}–$10^{11}\,{\rm M}_{\odot}$, the ones of interest to this work.

Satellites continue forming stars according the their availability of residual gas, and at the rate specified by their specific star formation at infall as (Karim et al. 2013; Peeples & Somerville 2013)

$${\rm SSFR} = \frac{0.0324}{M_{\rm star}}(1+z)^{3.45}\left(\frac{M_{\rm star}}{10^{11}\,{\rm M}_{\odot}}\right)^{0.65}\ {\rm Gyr}^{-1}. \quad (12)$$

Note that our simple star formation prescription for satellites does not take into account any detailed treatment of stellar feedback during the life of the satellite, but simply prolongs in time the physical conditions at infall. In other words, we safely assume that the SSFR associated with the galaxy is the 'equilibrium one', result of the balance between gas infall and feedback.

Finally, for completeness, we include in the scaling relations initializing centrals and infalling satellites, a lognormal scatter of 0.15 dex around the median stellar mass (Moster et al. 2013), a mean 0.2 dex in the gas fraction (Stewart et al. 2009), a 0.1 dex in in the input $f_{\rm orb}$ parameter (Khochfar & Burkert 2006), a 0.1 dex in SSFR (Karim et al. 2011) and a median 0.1 dex in disc radius (Somerville et al. 2008).

To summarize, a SHAM model empirically initializes central galaxies as stellar, gas-rich discs. Satellites are assigned all the properties of a central galaxy living in a typical halo of the same mass of the host at the epoch of infall. Satellite galaxies can then be quenched, and/or stripped, and/or continue to form stars according to their SSFR. Centrals instead at all epochs continue to be updated along the main progenitor halo in the dark matter merger trees until a merger occurs.

3.4.1 *Variants to the reference SHAM*

As discussed above, galaxy evolution via semi-empirical models is restricted to fewer basic input parameters. This in turn allows a more direct and transparent understanding of the impact of any additional input physical process. In the following when comparing with the data, we will thus also discuss several variations to our reference SHAM, alongside with the more extensive SAMs discussed above.

More specifically, we will present the following set of key variants to the reference SHAM.

(i) A SHAM characterized by $f_{\rm orb} = 0$ (keeping a dispersion of 0.3 dex), i.e. assuming on average parabolic orbits.

(ii) A SHAM with $f_{\rm orb} = 0$, with gas dissipation in major mergers following equation (3).

(iii) A SHAM with $f_{\rm orb} = 0$, and satellites undergoing fast quenching after infall (i.e. 0.5 Gyr instead of the 2 Gyr of the reference model).

(iv) A SHAM with $f_{\rm orb} = 0$, which adopts a dynamical friction time-scales a factor of 1/3 less than the one by McCavana et al. (2012), used as a reference in all other SHAM models.

(v) A SHAM equal to the reference one, also including an empirically motivated mass-dependent stellar and gas stripping, parametrized as (Cattaneo et al. 2011)

$$F_{\rm strip} = (1-\eta)^{\tau}, \quad (13)$$

with $\tau = t_{\rm df}/t_{\rm dyn}$ being the ratio between the dynamical friction and dynamical time-scales. As detailed below, the exact consumption of gas via star formation during infall is nearly fully degenerate with the amount of stripping assumed in the models. We will discuss the value adopted for the η parameter in the next sections. Stellar stripping does not only affect stellar mass but also disc size. We assume that, on average, the disc during its evolution always strictly follows an exponential profile, with its central density obeying the relation $\Sigma = M_{\rm disc}/2\pi Rs$. Thus we assume the central density to be conserved at each stripping event and update stellar and disc radius accordingly.

Finally, although we include in all SHAMs mild bar instabilities following equation (7), we find in our semi-empirical models the latter process to a very minor role in the build-up of massive bulges. We can thus safely refer to our SHAMs as models with negligible disc instabilities. Given that the full range of disc instabilities from moderate, to strong, to very strong ones, have already been extensively covered by the reference SAMs discussed above (G11/S13, MORGANA and B06, respectively), we will not further pursue this issue in SHAMs.

4 RESULTS

4.1 Comparison strategy: sample selection and treatment of observational errors

In our comparison between galaxy models and data we will mainly focus on *central* galaxies. Central galaxies are the ones believed to be the most affected by mergers, especially at later times, and

Downloaded from http://mnras.oxfordjournals.org/ at INAF Trieste (Osservatorio Astronomico di Trieste) on January 8, 2016

should thus be those type of systems for which any environmental dependence is in principle maximized. We will anyhow briefly discuss satellites in Appendix B.

We stress that in this work we preferentially select galaxies based on their morphology. We are in fact here mainly interested in studying the global structure of galaxies as a function of stellar mass and environment, and thus do not attempt to impose any further cut in, e.g. star formation rate, to limit the selection to passive galaxies. Nevertheless, we note that the most massive local massive and central galaxies of interest here are mostly passive. We have checked, for example, that the distributions predicted by the G11 and S13 models are nearly unchanged if we restrict to very massive galaxies with a SSFR below, e.g. $<0.01\,\mathrm{Gyr}^{-1}$. This is in line with the observational evidence reviewed in Section 2 which suggests the null environmental dependence to be independent of the exact selection adopted.

When discussing environmental trends (Section 4.5), we chose to consider in our analysis all early-type galaxies more massive than $\log M_1/\mathrm{M}_\odot > 11.2$, an interval of stellar mass which includes galaxies up to a few $\log M_{\rm star}/\mathrm{M}_\odot \sim 12$. This solution allows the bin to be sufficiently large not to be dominated by errors in stellar mass estimates (e.g. Huertas-Company et al. 2013a), and at the same time to maximize the statistics in about three decades of host halo mass (cf. right-hand panel of Fig. 1), from the field/small group scale with $\log M_{\rm halo}/\mathrm{M}_\odot \gtrsim 12.5$, to massive clusters with $\log M_{\rm halo}/\mathrm{M}_\odot \lesssim 15$. We stress, however, that varying the amplitude of the stellar mass interval does not qualitatively impact the general trends discussed in this work (see, e.g. Huertas-Company et al. 2013a,b).

When comparing model predictions to data we will start off by showing the raw model predictions. However, we are here interested to probe not only the median correlations, but even more to understand the scatters around these relations, and how the latter depend on environment. It is thus essential to take into account observational errors, to properly deal with residuals around median relations.

To achieve this, we closely follow the results of Bernardi et al. (2013) and Meert, Vikram & Bernardi (2013). By fitting a series of simulations to an unbiased SDSS galaxy sample, Meert et al. (2013) found that single Sérsic models of SDSS data are usually recovered with a precision of 0.05–0.10 mag and 5–10 per cent in radius. Bernardi et al. (2013) then pointed out that significant systematics can be induced in the derivation of total luminosities and half-light radii R_e of massive galaxies residing in denser environments, mainly due to issues linked to sky subtraction and exact choice of fitting light profile. Detailed simulations (Meert et al. 2013) have shown that up to 0.5 mag (i.e. 0.2 dex in luminosity/stellar mass) of systematic error could affect the measurement of the total light competing to the most massive galaxies, inducing a nearly parallel error in the estimate of R_e. The latter systematics could easily affect the final estimate of stellar mass at the same order of other independent large systematics arising from, e.g. different assumptions about the stellar mass-to-light ratio.

We thus first assigned independent Gaussian *statistical* errors to stellar masses and sizes with (typical) dispersions (Huertas-Company et al. 2013b) of 0.2 and ∼0.1 dex, respectively [the error in size is slightly luminosity dependent following Bernardi et al. (2013), but simply keeping it constant to 0.1 dex does not minimally alter the results]. On top of the statistical uncertainties, to reflect the results of the simulations of Bernardi et al. (2013), we then added a *systematic* variation in predicted stellar mass. The latter is computed as follows. We first transform each stellar mass to luminosity following the mass–luminosity relation of Bernardi et al. (2013). To each luminosity we then assign the maximum possible systematic error following the largest luminosity-dependent correction given in fig. 1 of Bernardi et al. 2013, which amounts to $\Delta M_r \sim 0.014$ for $M_r \gtrsim -21$ and progressively growing to $\Delta M_r \gtrsim 0.3$ for $M_r \sim -23$, up to $\Delta M_r \gtrsim 0.6-0.7$ for $M_r \sim -24$. All magnitudes are then converted back to luminosities using the same mass–luminosity relation. The corresponding size is then updated by the total change in stellar mass/luminosity as $\Delta\log R_e \equiv \Delta\log L$.

We here note that a correlation of the type $\Delta\log R_e \sim \Delta\log L$ has also been confirmed by previous studies (e.g. Saglia et al. 1997; Bernardi et al. 2003). Nevertheless, other types of correlation errors between luminosity and size may be possible. For example, if different measurements reach to different surface brightness levels, then one could expect a correlation closer to $\Delta\log R_e \sim 0.5\Delta\log L$. We have verified, however, that our main results and conclusions are unaffected by the inclusion of the latter (weaker) correlation. We also acknowledge that, in principle, errors among observables such as stellar mass and size may not be fully correlated. For example, the error in stellar mass will also depend on other factors not necessarily linked to light profile's issues, such as the choice of templates or varying IMF (see, e.g. discussion in Bernardi et al. 2013, and references therein). Overall, assuming null or maximal correlation among errors will bracket the full range of possibilities.

Halo masses in the catalogue by Yang et al. (2007), adopted for reference in this work, are also maximally correlated to stellar masses via abundance matching between the total stellar mass

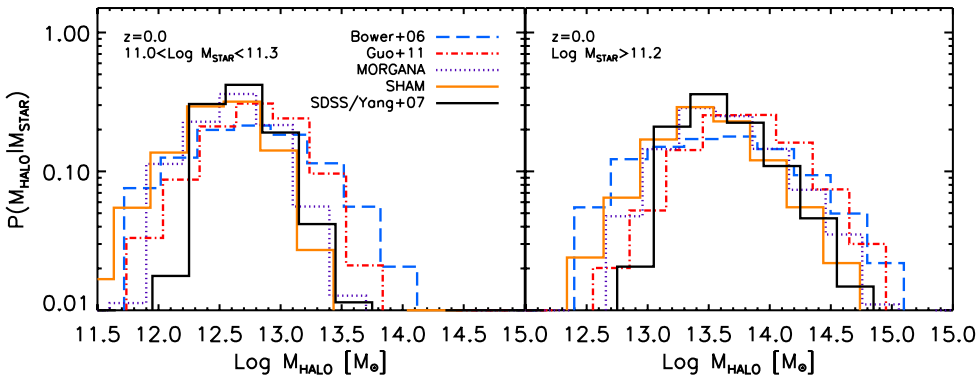

Figure 1. Predicted halo mass distributions for central galaxies of stellar mass in the range $11.0 < \log M_{\rm star} < 11.3$ (left) and $\log M_{\rm star} > 11.2$ (right), for different galaxy formation models, as labelled. The solid, black lines are the corresponding distributions for central early-type galaxies in SDSS (see the text for details). All predicted and observed distributions are broad, covering about two orders of magnitude in halo mass, if not more.

Downloaded from http://mnras.oxfordjournals.org/ at INAF Trieste (Osservatorio Astronomico di Trieste) on January 8, 2016

function of the groups and clusters, and the halo mass function of dark matter haloes. Following Huertas-Company et al. (2013b), in order to quantify the maximum propagated error in halo mass as a function of variation in the stellar mass of the central galaxy, we take advantage of the full Millennium simulation. We compute the stellar mass function of central galaxies in the Guo et al. (2010) model with and without systematic plus statistical errors, and for each case compute the corresponding median relation with halo mass via abundance matching with the halo mass function. This provides the median, stellar mass-dependent correction to host halo mass that must be applied to the Yang et al. catalogue when varying stellar masses. We remark that both the stellar mass function and cosmology used in Yang et al. (2007) differ a little with respect to the ones in the Millennium data base, but we expect these changes to have minimal impact in our computations given that we are here mainly interested in the median shift in halo mass, consequent to a variation in stellar mass, not in its absolute value.

We should also point out that assigning halo masses to galaxies via abundance matching could alter both the slope and intrinsic scatter in the true stellar mass–halo mass relation. Nevertheless, Huertas-Company et al. (2013b) proved that environmental dependence in the local Universe is not present even when adopting *fully independent* cluster mass measurements. In the specific, they showed that field massive galaxies share very similar size distributions to equally massive counterparts residing in 88 low-z clusters from Aguerri, Sánchez-Janssen & Muñoz-Tuñón (2007), with dynamically mass measurements obtained from the velocity distribution of spectroscopically confirmed galaxy members. We will thus present and discuss Monte Carlo simulation results in which we also allow the error on host halo mass to be fully uncorrelated to other quantities (though continuing to force maximal correlation between size and stellar mass).

4.2 Broad halo distributions at fixed stellar mass

Before discussing sizes and their connection to environment, it is clearly instructive to investigate the predictions of models with respect to the distributions of stellar masses in different environments, that hereby we physically identify with host group/cluster halo masses.

We first show in Fig. 1 the results obtained from the B06, G11, MORGANA and SHAM models (blue/long-dashed, red/dot–dashed, violet/dotted and solid/orange histograms, respectively). The left-hand panel shows the distributions in host halo mass for central galaxies within a factor of 2 in stellar mass, $11 < \log M_{\rm star} < 11.3$, while the right-hand panel reports the distributions for galaxies with $\log M_{\rm star}/{\rm M}_{\odot} > 11.2$, the latter being the actual stellar mass interval taken as reference for our study below (see Section 4). All models predict large distributions of halo masses at fixed bin in stellar mass. Even for relatively narrow bins in stellar mass of a factor of 2 (left-hand panel), models redistribute galaxies along broad ranges of hosts, differing by factors of $\gtrsim$50–100 in halo mass. Most models are also in broad agreement with the halo mass distributions inferred from the empirical sample (solid, black lines), obtained, we remind, by cross-correlating the early-type galaxy population in SDSS with the Yang et al. catalogue.

The analysis in Fig. 1 is restricted to central galaxies only, but satellites cover even broader halo mass distributions. More generally, we find the broadening to be independent of the exact stellar mass bin considered, or the exact B/T threshold chosen (here we set $B/T > 0.5$), or the type of galaxy considered (i.e. central or satellite), as long as the analysis is restricted to massive galaxies

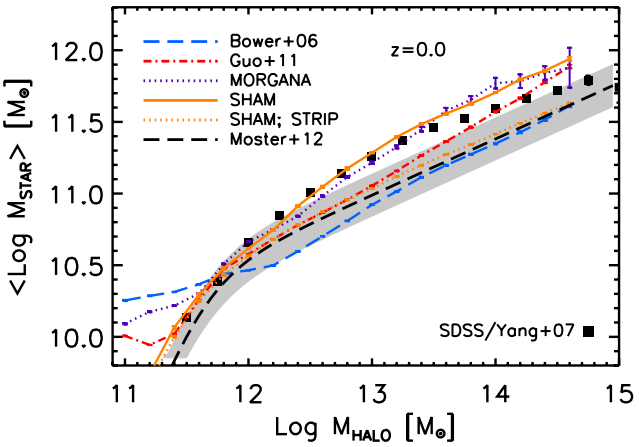

Figure 2. Predicted median stellar mass at fixed halo mass for central galaxies for all the reference models presented in Fig. 1, as labelled, at redshift $z = 0$. Models predict different stellar mass–halo mass relations, despite tuned to match the same stellar mass function, at least in the local Universe. The long dashed, black lines are the $M_{\rm star}$–$M_{\rm halo}$ relation derived by Moster et al. (2013) from abundance matching techniques shown along with their 1σ dispersion (grey bands). The solid squares are the median $M_{\rm star}$–$M_{\rm halo}$ relation competing to central SDSS early-type galaxies, derived from the Huertas-Company et al. (2013b) galaxy catalogue matched to the Yang et al. (2007) halo catalogue (see the text for details).

($\log M_{\rm star} \gtrsim 10^{11}\,{\rm M}_{\odot}$). In other words, all the galaxy formation models in this work share the view that galaxies of similar stellar mass can emerge from different environments and may have thus undergone different growth histories. This basic feature motivates a systematic study of galaxy structural properties at fixed stellar mass in different environments. Despite small differences in the broadness of halo distributions at fixed stellar mass (with the B06 predicting the largest dispersions), all models roughly share distributions comparable to the empirical ones. This shows that all models predict a median halo mass at fixed bin of stellar mass in agreement with the data. This is not entirely unexpected, given that the models have been tuned to broadly reproduce the local stellar mass function.

Fig. 2 shows instead the median stellar mass as a function of halo mass. Due to the large scatters involved, the latter is not equivalent to the median halo at fixed stellar mass. It is intriguing that only two models (MORGANA and SHAM) well agree with the SDSS/Yang et al. data (filled squares), while all the others lie somewhat below in stellar mass at fixed halo mass. The latter models are discrepant at the high-mass end by a systematic factor of $\sim$2 with the Yang et al. results, but in better agreement with $z = 0$ stellar mass–halo mass relation worked out by Moster et al. (2013) via abundance matching techniques (long-dashed line with its 1σ scatter shown as a grey area). Empirical estimates of the stellar mass–halo mass relation still in fact disagree by a factor of a few (e.g. Behroozi, Conroy & Wechsler 2010; Rodríguez-Puebla, Drory & Avila-Reese 2012), or possibly even more according to some studies (e.g. Neistein et al. 2011; Yang et al. 2012), with galaxy evolution models predicting a similar degree of discrepancy. What is relevant to this work is anyway exploring structural differences in halo mass at *fixed* bin of stellar mass, so factors of $\lesssim 2$ disagreement in scaling relations are not a major limitation for the present study.

We conclude the section by emphasizing that even if (proto) galaxies in the SHAM by construction are forced to lie on the Moster et al. (2013) relation (Section 3.4), the resulting $M_{\rm star}$–$M_{\rm halo}$

Downloaded from http://mnras.oxfordjournals.org/ at INAF Trieste (Osservatorio Astronomico di Trieste) on January 8, 2016

is predicted to be displaced upwards with respect to the $z = 0$ Moster et al. relation by up to a factor of $\sim$2 at high stellar masses. It has already been pointed out that mergers between galaxies initialized on the $z > 0$ abundance matching $M_{\rm star}$–$M_{\rm halo}$ relation can scatter upwards the newly formed ellipticals (e.g. Monaco et al. 2006; Cattaneo et al. 2011; Zavala et al. 2012). This is an effect due to the slow evolution in the empirical $M_{\rm star}$–$M_{\rm halo}$ relation at late times, compared to the sudden increase in stellar mass due to mergers. The addition of significant stellar stripping in the infalling satellites can definitely limit this tension and bring most of the outliers back on the empirical relation at $z = 0$ (e.g. Monaco et al. 2006; Cattaneo et al. 2011). We prove this by showing how the version of the SHAM inclusive of stellar stripping with $\tau = 0.25$ in equation (13), well matches the $z = 0$ Moster et al. (2013) relation (dotted, orange lines in Fig. 2). In the following we will continue to consider the SHAM without stellar stripping (solid, orange lines) as our reference model, as it is in better agreement with the empirical halo–galaxy catalogue used as observational constraint, although we will mention the model with stripping where relevant.

4.3 B/T distributions at fixed stellar mass bin

In order to properly compare size distributions in different environment, it is necessary to first understand what the predictions of the models are with respect to morphology, at least in the range of high stellar masses of interest here.

Fig. 3 shows that all models predict quite a narrow distribution for B/T, with massive central galaxies mostly gathered around $B/T \gtrsim 0.8$ (all distributions are normalized to unity). Significant, long tails to the lowest values of B/T are however present, especially in less massive haloes with $M_{\rm h} \lesssim 3$–$5 \times 10^{12} {\rm M}_{\odot}$. In general, minor mergers are responsible for creating small bulges in these models with $B/T \sim 0.1$–0.3. However, disc instabilities, when present, inevitably drive the growth of larger bulges. The exact resulting distribution of B/T is clearly dependent on the strength/type of the disc instability, and it is mainly relevant at intermediate to low stellar masses, as also identified by previous studies (e.g. De Lucia et al. 2011; Shankar et al. 2013).

Although the exact shape of the B/T distribution characterizing each model is the result of a complex interplay among a variety of different physical processes (e.g. De Lucia et al. 2011), we can still capture some basic trends. The B06 and MORGANA models (left-hand panels), characterized by the strongest disc instabilities, tend to produce quite broad B/T distributions in the lowest mass host haloes. This is not unexpected, as the regime where the condition in equation (4), of high disc circular velocities and corresponding low host halo velocities, is most easily met in lower mass haloes with massive galaxies. The G11 model, with the mildest disc instabilities (cf. Section 3), predicts instead more Gaussian-shaped distributions for the low-B/T objects, peaked around $B/T \sim 0.4$–0.7. The SHAM, with practically negligible disc instabilities, tends to predict even lower fractions of low-B/T galaxies.

Fig. 3 hints towards the fact that all hierarchical models considered in this work predict massive galaxies in the local Universe to be bulge dominated with $B/T \gtrsim 0.8$. More generally, we checked that all models predict a rising fraction of central galaxies with $B/T > 0.5$ as a function of stellar mass in good agreement with the data, although models with stronger disc instabilities tend to overproduce the fraction of bulge-dominated galaxies at stellar masses $M_{\rm star} \lesssim (1$–$2) \times 10^{11}$ M$_{\odot}$ (see also Wilman et al. 2013). What is relevant to our present discussion is that all models agree in predicting a dominant fraction of galaxies with high stellar masses $\gtrsim 10^{11}$ M$_{\odot}$ and large bulges built mainly via mergers. However, most models also predict a more or less pronounced population of galaxies with

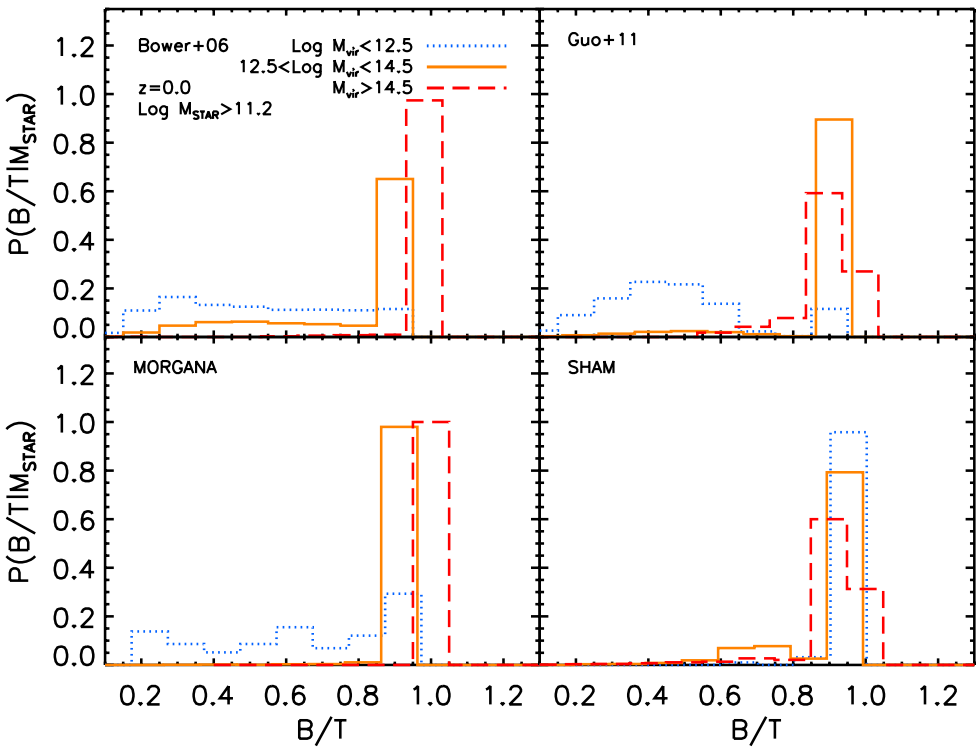

Figure 3. Predicted B/T distributions for central galaxies with stellar mass in the range $\log M_{\rm star}/{\rm M}_{\odot} > 11.2$ residing in different bins of halo mass, $\log M_{\rm h}/{\rm M}_{\odot} < 12.5$, $12.5 < \log M_{\rm h}/{\rm M}_{\odot} > 14.5$ and $\log M_{\rm h}/{\rm M}_{\odot} > 14.5$, for the four reference models, as labelled.

Downloaded from http://mnras.oxfordjournals.org/ at INAF Trieste (Osservatorio Astronomico di Trieste) on January 8, 2016

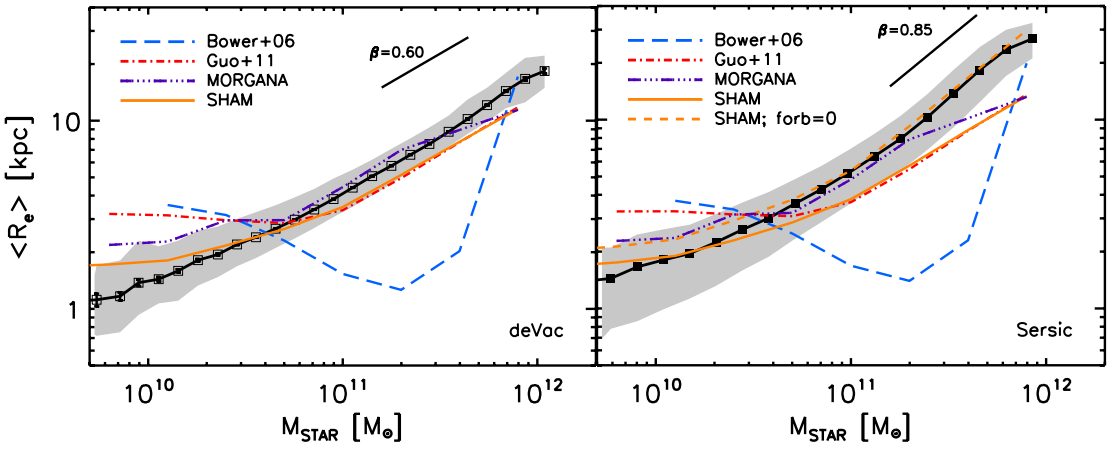

Figure 4. Predicted median size as a function of stellar mass for central galaxies with $B/T > 0.5$ for all the models presented in Fig. 1, as labelled. The left-hand panel shows predictions converted from 3D to 2D quantities using a constant factor assuming $n = 4$ for all galaxies, and the open squares represent the relation derived by Bernardi et al. (2011b) using *cmodel* magnitudes. The right-hand panel shows predictions obtained by associating to each simulated galaxy an empirical n. In this panel we also include a version of the SHAM characterized by having $f_{\rm orb} = 0$ in equation (2) (orange, dotted line). The filled squares are the median size–stellar mass relation derived by Bernardi et al. (2013), using Sérsic profiles. The grey areas in both panels mark the 1σ uncertainty regions in the data. The Sérsic data are better reproduced by models having $f_{\rm orb} = 0$.

still massive bulges ($B/T \gtrsim 0.5$) residing at the centre of lower mass haloes grown mainly via disc instabilities. This in turn, we will see, has a non-negligible impact on the environmental dependence of sizes in lower mass haloes.

4.4 The median size–stellar mass relation

We begin our study of early-type galaxy structural properties by showing in Fig. 4 a general comparison among the median size–stellar mass relations predicted by the reference galaxy evolutionary models against the data.[6] For the latter, we show two estimates of the R_e–$M_{\rm star}$ relation. The filled squares (right-hand panel) represent the median size–mass relation from the data discussed in Section 2. Sizes are based on Sérsic profiles (Sérsic 1963) taken from Bernardi et al. (2013). The open squares (left-hand panel) represent instead the relation derived for a SDSS sample of early-type galaxies by Bernardi et al. (2011b) using *cmodel* magnitudes, a combination of a de Vaucouleurs (1948) and exponential profiles, as discussed in Bernardi et al. (2010). The latter relation was calibrated on a sample of early-type galaxies with no restriction on centrals. More generally, the sample used by Bernardi et al. (2011b) is not exactly matched to the one in the right-hand panel, but this is irrelevant to our present discussion. We here present both relations compared to models to simply emphasize the typical systematic observational uncertainties that inevitably affect size measurements. As anticipated in Section 4.1, fitting galaxy with different model profiles can yield different sizes at fixed luminosity/stellar mass up to a systematic variation of $\gtrsim$50 per cent, as seen in Fig. 4, when comparing de Vaucouleurs (left-hand panel) and Sérsic (right-hand panel) profiles. For the rest of the paper we will refer only to sizes derived from Sérsic profiles, as they are a better fit to the light profiles of massive galaxies (Bernardi et al. 2013, and references therein).

As in S13 when comparing model 3D half-mass radii R_H to measured 2D projected half-light radii R_e, we assume that light traces mass and convert R_H to R_e using the tabulated factors from Prugniel & Simien (1997), i.e. $R_e \approx 2S(n)R_H$, with the scaling factors $S(n)$ dependent on the Sérsic index n. Our mock galaxy catalogues lack predictions on the evolution of n competing to each galaxy. In principle, it is possible to predict a Sérsic index a priori from the models (e.g. Hopkins et al. 2009), but this relies on several additional assumptions on the exact profile and its evolution with time of the dissipational and dissipationless components, that the true advantage with respect to simply empirically assign a Sérsic index at $z = 0$ is modest. We thus prefer to stick to a minimal approach with the least set of physical assumptions and corresponding number of parameters.

We first compute 3D sizes from energy conservation arguments, as detailed in Section 3. Given that we are here mainly interested in bulge-dominated massive galaxies, we could simply set $n = 4$ [i.e. $S(4) = 0.34$ from table 4 of Prugniel & Simien 1997, an average value characterizing such galaxies (e.g. Bernardi et al. 2013; Huertas-Company et al. 2013a, and references therein). The left-hand panel of Fig. 4 shows predictions converted from 3D to 2D quantities using a constant $n = 4$ for all galaxies. The right-hand panel of Fig. 4 shows instead predictions obtained via a mass-dependent n, in which each mock galaxy has been assigned an index n from our empirical n–$\log M_{\rm star}$ relation (Section 2). We find the outputs to be so similar that including or not a mass-dependent conversion factor $S(n)$ makes little difference to our results below. For consistency with the data, in the following we will continue adopting the mass-dependent Sérsic correction as our reference one.

There are several general noteworthy features in Fig. 4. First, models, despite the different details in computing galaxy stellar masses and sizes, predict quite similar R_e–$M_{\rm star}$ relations, both in shape and normalization, especially for $M_{\rm star} \gtrsim 3 \times 10^{10}\,{\rm M}_\odot$. The broad agreement with the data is also reasonable, most models lie within the 1σ uncertainties of sizes at fixed stellar mass (dotted lines), except for the B06 model, which significantly diverges

[6] Median sizes are computed from the 50 per cent percentile of the full statistical distribution of galaxies competing to each bin of halo mass considered (for the SHAM, as discussed in Section 3.4, the statistical distribution is weighted by the number of effective haloes considered, although neglecting such extra weighting makes little difference). The error on the median is computed by dividing the 1σ uncertainty of the same distribution by the square root of the number of galaxies in that bin of halo mass.

Downloaded from http://mnras.oxfordjournals.org/ at INAF Trieste (Osservatorio Astronomico di Trieste) on January 8, 2016

from them. This has been extensively discussed by González et al. (2009) and Shankar et al. (2010b), and it can be ascribed to some possibly wrong initial conditions, as a similar behaviour is present also at higher redshifts. In particular, varying their input parameters does not ameliorates the match, although an improvement can be achieved by switching off adiabatic contraction (González et al. 2009). Despite being the B06 model highly divergent with respect to the global size–stellar mass relation, for completeness, we will continue keeping it as one of our reference models, even when discussing environmental dependence.

Irrespective of the exact 3D-to-2D conversion adopted, models fall short (at the $\sim 2\sigma$ level) in reproducing the exact normalization of the Sérsic size–mass correlation at masses $M_{\rm star} \gtrsim 1$–$2 \times 10^{11}\,{\rm M}_{\odot}$ (right-hand panel), indicative of a more profound cause of discrepancy. The short-dashed, orange line shows the prediction of the SHAM model with the same specifications as the reference one but with $f_{\rm orb} = 0$ (i.e. negligible orbital energies, parabolic orbits). As anticipated by S13, this variation in the merging model effectively produces larger sizes for the same stellar mass because each merger event is more efficient in enlarging the central galaxy (equation 2). More massive galaxies which are the most affected by mergers, will proportionally be larger resulting in an overall steepening of the size–stellar mass relation and a significantly better agreement with the data (cf. solid/orange and short-dashed/orange lines). The predicted slope of the size–stellar mass relation at high masses steepens from $\beta \sim 0.6$ (left-hand panel) to $\beta \sim 0.8$–0.9 (right-hand panel) when setting $f_{\rm orb} = 0$.

In Fig. 5 we report the predicted size–stellar mass relation for the different SHAMs introduced in Section 3.4.1, with null input median orbital energy, with gas dissipation, with fast satellite quenching and with a shorter dynamical friction time-scale. Analogously to what emphasized with respect to Fig. 4, SHAM models with $f_{\rm orb} = 0$ share a slope at the massive end of $\beta \sim 0.8$–0.9, in better agreement with the observed one, while $\beta \sim 0.6$ for models with $f_{\rm orb} > 0$. While for consistency with the other models, we will continue using $f_{\rm orb} > 0$ in the SHAM reference model, we will extensively discuss models characterized by $f_{\rm orb} = 0$ which represent a better match to the Sérsic data.

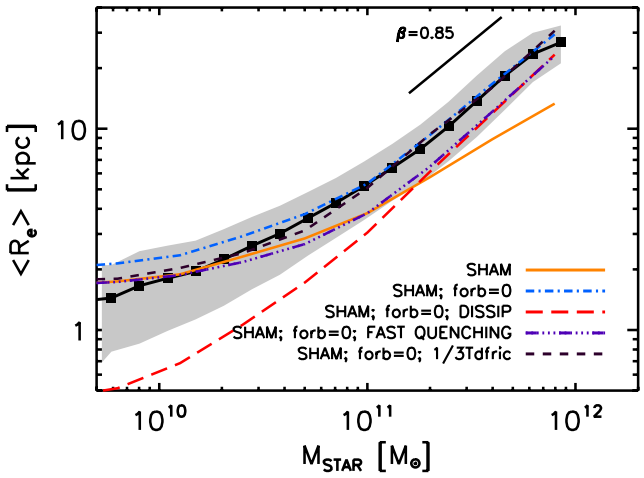

Figure 5. Predicted median size–stellar mass relation for different versions of the SHAM model, as labelled, compared to data (solid line with grey area marking the 1σ uncertainty region). All models predict similar scaling relations especially at the massive end, within a factor of $\lesssim 2$ in normalization. The predicted slope is around $\beta \sim 0.8$–0.9 for all models with $f_{\rm orb} = 0$, and closer to $\beta \sim 0.60$ for models with $f_{\rm orb} > 0$.

Irrespective of details on the exact galaxy profile, the different steepening in the size–stellar mass relation for different models could be qualitatively probed directly from equation (2). As already sketched several times in the literature (e.g. Bernardi 2009; Naab et al. 2009; Shankar & Bernardi 2009, and references therein), we can in fact write the increase in radius due to mergers as

$$\frac{R_{\rm new}}{R_1} = \frac{(1+f)^2}{(1+f^2/\eta + kf/(1+\eta))}, \tag{14}$$

with $f = M_2/M_1$, $\eta = R_2/R_1$ and $k = f_{\rm orb}/c$. For simplicity, considering a merger history dominated by (very) minor mergers with $f^2 \ll f \ll 1$, and $\eta \approx f$ we can set, after some approximations,

$$\beta = \frac{\Delta \log R}{\Delta \log M_{\rm star}} = \frac{\Delta R}{R}\frac{M_{\rm star}}{\Delta M_{\rm star}} \approx \frac{f(1-k)}{(1+kf)}\frac{1}{f}, \tag{15}$$

which yields $\beta \gtrsim 0$, 1 for $k \sim 1$, 0 respectively. Clearly the latter approximations are very basic and cannot capture the full complexities behind galaxy merger histories, but nevertheless clearly highlight how the slope of the size–stellar mass relation can easily steepen for lower values of $f_{\rm orb}/c$. In other words, the slope of the size–stellar mass relation at high masses in hierarchical models is more a consequence of the *type* rather than the number of galaxy mergers.

It is evident from Figs 4 and 5, that despite the different input physical assumptions, most of the models predict similar size–stellar mass relations within the 1σ uncertainties of the data (grey bands). The differences are within a factor of $\lesssim 2$ at high stellar masses $\gtrsim 10^{11}{\rm M}_{\odot}$, the ones of interest here. The predicted behaviour among different models below $M_{\rm star} \lesssim 10^{11}{\rm M}_{\odot}$ is instead somewhat varied. Most of the SAMs in Fig. 4 predict a more or less pronounced flattening at lower masses, while the SHAMs in Fig. 5 tend to mostly align with the data, except for the SHAM with gas dissipation which tends to progressively fall below the data at low stellar masses. S13 discussed that the low-mass end shape of the resulting size–stellar mass relation depends, among other factors, on the exact slope of the underlying $M_{\rm star}$–$M_{\rm halo}$ relation in the same stellar mass range, thus explaining part of the discrepancies among different models. Furthermore, as discussed by Hopkins et al. (2009) and Covington et al. (2011), gas dissipation can effectively shrink the sizes of lower mass bulges, remnants of gas richer progenitors. S13 showed that this mechanism can indeed significantly ameliorate the match to the data in the G11 model, entirely removing the flattening in sizes at low masses. On the other hand, the SHAM with gas dissipation tends to drop at low masses more rapidly than the G11 model with gas dissipation (see full discussion and related figures in S13), possibly due to the different $M_{\rm star}$–$M_{\rm halo}$ relations, input gas fractions, and detailed treatment of satellites.

Some properly fine-tuned disc regrowth/survival after a gas-rich major merger (e.g. Puech et al. 2012; Zavala et al. 2012) could boost the total sizes of low-mass galaxies, thus improving the match between the data and the SHAM with gas dissipation (but then worsening the good one with the G11/S13 model). Bernardi et al. (2013) have indeed recently stressed that the contribution of a disc component in early-type samples becomes increasingly more important below $\lesssim 10^{11}\,{\rm M}_{\odot}$, while the size of the bulge component becomes progressively more compact. The latter may then require on one side gas dissipation to get enough compact bulges (see also discussion in Hopkins et al. 2009), and on the other possibly some properly fine-tuned disc regrowth (e.g. Puech et al. 2012) to recover the disc components measured in these galaxies. A full treatment of the general impact of gas dissipation and/or disc regrowth models in low-mass galaxies is beyond the scope of this work, and in the

Downloaded from http://mnras.oxfordjournals.org/ at INAF Trieste (Osservatorio Astronomico di Trieste) on January 8, 2016

following we will mainly focus on the impact of gas dissipation alone in the context of environmental dependence of very massive spheroids.

To summarize, Figs 4 and 5 prove how the size–stellar mass relation by itself may not represent a major discriminant for determining the success of a galaxy evolution model with respect to another, especially for bulge-dominated galaxies above $\gtrsim 10^{11}$ M$_\odot$. In the following, we will discuss how galaxy sizes coupled with the notion on their environment, defined here as the host total halo mass, can provide useful additional physical insights.

4.5 Environmental trends

To start off with, Fig. 6 reports for both models and data, the median sizes competing to galaxies of similar stellar mass but living in different environments, in the specific, at the centre of haloes of mass $\log M_{\rm halo}/{\rm M}_\odot < 13$, $13 < \log M_{\rm halo}/{\rm M}_\odot < 14$ and $\log M_{\rm halo}/{\rm M}_\odot > 14$ (marked by dotted, solid and long dashed lines, respectively). Only bins with at least 20 galaxies are retained in this plot.

While the observed size–stellar mass relation seems to be quite ubiquitous in all environments, there is a net tendency for models to predict larger galaxies in more massive haloes. This tendency is marginal for the models on the right-hand panels, while significantly more pronounced in the models reported in the left-hand panels. In the specific, the reference SHAM predicts a rather moderate environmental dependence of up to ∼30 per cent at fixed stellar mass, the G11 model up to a factor of ∼2, the MORGANA up to $\lesssim 3$, and the B06 model up to even a factor of $\lesssim 5$ in the most massive bins. The latter two models, we recall, are the models characterized by the strongest disc instabilities (cf. Section 3), thus possibly suggesting that this physical process may contribute to such a trend.

4.5.1 *What is driving the trend?*

As extensively discussed in Section 4.4, most of the models considered in this work align within the 1σ uncertainty with the high-mass end of the local size–stellar mass relation. Moreover, a simple change in one of the parameters such as, e.g. $f_{\rm orb}$, can help to further fine tune the models to match the data. Thus, both the slope and normalization of the R_e–$M_{\rm star}$ relation cannot really be effective in distinguishing among the successful models. On the other hand, the residuals around the median relation can provide useful additional hints to constrain the models, as proven below.

Here we re-propose the same argument of Fig. 6 but in a different format. Following, e.g. Cimatti et al. (2012) and Newman et al. (2012), we first select galaxies in a given bin of stellar mass in the range M_1 and M_2 and then normalize their sizes following the relation:

$$\log \gamma = \log R_e + \beta(11 - \log M_{\rm star}). \quad (16)$$

Equation (16) allows us to weight each size by its appropriate stellar mass, according to its (median) position on the size–mass relation. This way galaxies within the bin, which appear larger/smaller because more/less massive, are properly renormalized removing any spurious effect in the study of residuals around the relation.

The slope β in equation (16) is then for each model self-consistently computed in the range of stellar mass $11.2 < \log M_{\rm star}/{\rm M}_\odot < 12$, the one of interest in this work (Section 4.1). As shown in Fig. 5, most of the models characterized

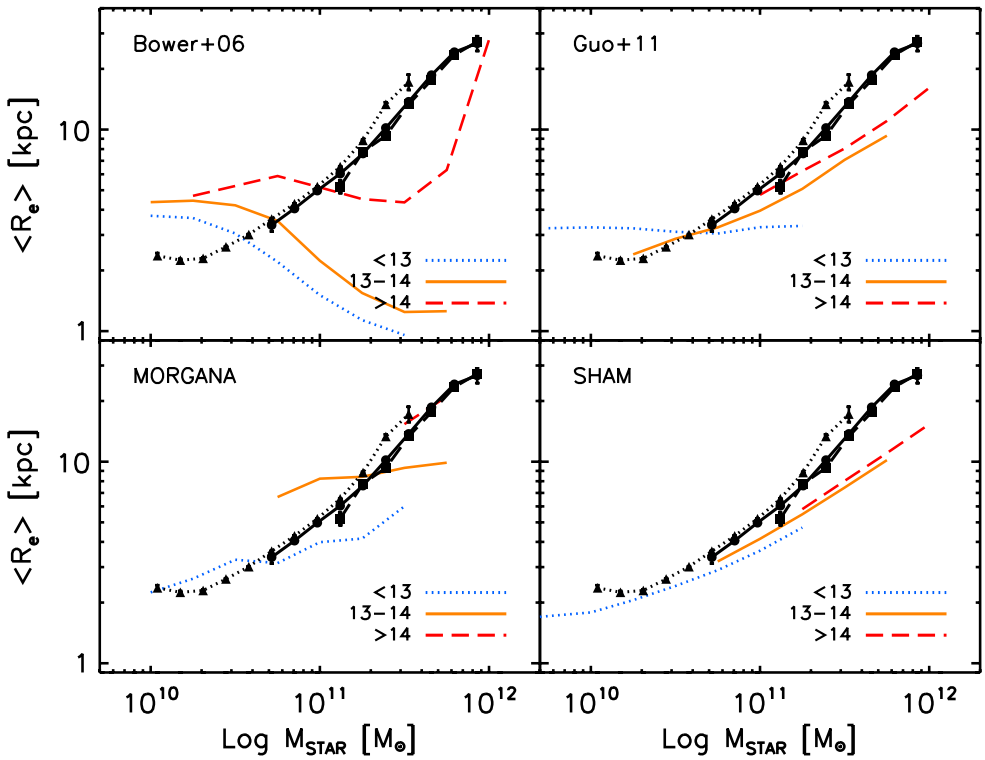

Figure 6. Predicted median size–stellar mass relation of central galaxies in different bins of halo masses, $\log M_{\rm halo}/{\rm M}_\odot < 13$, $13 < \log M_{\rm halo}/{\rm M}_\odot < 14$ and $\log M_{\rm halo}/{\rm M}_\odot > 14$, for different models, as labelled. Data (black lines with symbols) are as in Fig. 4, divided by the same bins of host halo mass as in the models. All models present a more or less pronounced variation up to a factor of $\lesssim 3$ of median size at fixed stellar mass, when moving from low- to high-mass haloes.

Downloaded from http://mnras.oxfordjournals.org/ at INAF Trieste (Osservatorio Astronomico di Trieste) on January 8, 2016

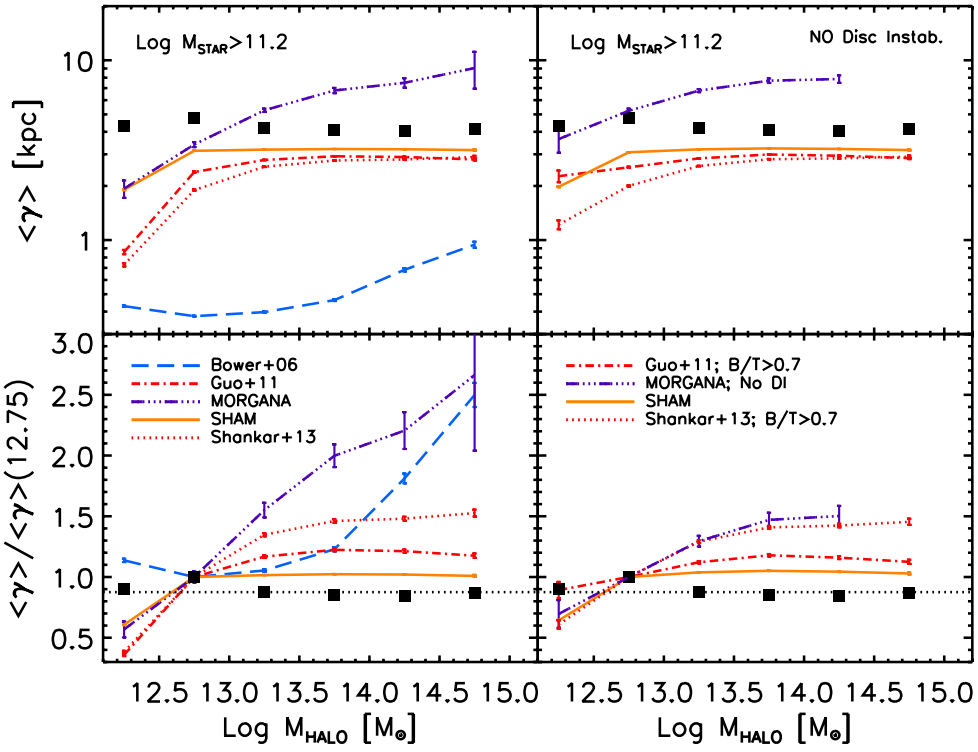

Figure 7. Fractional increase of median size in the stellar mass bin $\log M_{\rm star}/{\rm M}_{\odot} > 11.2$ and $B/T > 0.5$ for the different type of reference models discussed in Section 3, as labelled. Data have been discussed in Section 2. Models with weak or absent disc instabilities are favoured.

by $f_{\rm orb} = 0$, have a slope of $\beta \gtrsim 0.8$ in this mass range, in close agreement with the high-mass end slope present in the data. Models which also include gas dissipation in major mergers, e.g. one version of the SHAM and S13, are the ones characterized by the steepest relations at the massive end with $\beta \sim 0.9$ (cf. Fig. 5). All other galaxy models characterized by $f_{\rm orb} > 0$, tend to have a shallower slope of $\beta \sim 0.60$ (see Fig. 4).

Fig. 7 shows the predicted mass-normalized sizes γ as a function of host halo mass for all central galaxies with $B/T > 0.5$. Both the left- and right-hand panels comprise the outputs from the compilation of our reference models, the B06, G11, MORGANA and basic SHAM, as labelled. For completeness, we also add the predictions of the S13 model, introduced in Section 3.2, variation of the G11 model which, we remind, includes gas dissipation in major mergers and a value of $f_{\rm orb} = 0$.

To further highlight the true information on the residuals, we normalize each γ to one single value, thus removing the effect of the global median normalization in the R_e–$M_{\rm star}$ relation. In the lower panels of Fig. 7, median γ sizes have been divided[7] by the median γ competing to galaxies residing in haloes with mass in the range $12.5 < \log M_{\rm halo}/{\rm M}_{\odot} < 13.0$, to emphasize any difference in median size when moving from lower to higher mass haloes hosting central galaxies of the same stellar mass (which could in principle be induced by either larger galaxies at the centre of clusters, and/or more compact galaxies in the field).

In the left-hand panels a fast variation in the median γ by a factor of ∼1.5–3 is evident in most galaxy evolution models, when moving from field/groups to cluster scale host haloes. This behaviour is clearly at variance with the data which suggest a flat size distribution as a function of halo mass, as indicated by the horizontal, dotted line which marks the average normalized γ value in the data. The discrepancy between model predictions and data is at face value highly significant. The reference SHAM is the only one predicting a very mild variation, up to a factor of ∼1.3–1.5 or so, and nearly absent above haloes of mass $\log M_{\rm halo}/{\rm M}_{\odot} \gtrsim 13$. We will further discuss variations to the reference SHAM below. Here we highlight that models characterized by mergers, strong disc instabilities (B06 and MORGANA), and/or significant gas dissipation in (major) mergers (S13) predict, on the contrary, large discrepancies with the data.

To isolate the role of mergers with respect to that of disc instabilities, the right-hand panels of Fig. 7 show the same models but with null or minimal contribution from disc instabilities. To this purpose, we restrict the predictions of the G11 and S13 models to the subsamples of galaxies with $B/T > 0.7$, a limit above which it was shown that bulges grow mainly via mergers (see discussion in Shankar et al. 2013). In the same panels we also report a variation of the MORGANA model *without* any disc instabilities. We keep for reference the SHAM model, for which the contribution of disc instabilities is already negligible, as anticipated in Section 3.4.

It is interesting to note that in the absence of disc instabilities the environmental dependence is reduced in all models, in the sense that galaxies living in host haloes of mass $\log M_{\rm halo}/{\rm M}_{\odot} \lesssim 13$ tend to be larger than galaxies of comparable stellar mass and in the same haloes but lower B/T, while median sizes remain less affected beyond this halo mass scale. This behaviour is directly explained by the fact that disc instabilities (equation 4), most frequent in lower host dark matter haloes, are less efficient than mergers in producing large bulges of comparable mass, as anticipated in Section 3 (cf. equations 2 and 5). Overall, models in which bulges significantly

[7] We choose to normalize in the interval $12.5 < \log M_{\rm halo}/{\rm M}_{\odot} < 13.0$ as this is the lowest mass bin in halo mass retaining a significant number of massive galaxies (see Fig. 1).

Downloaded from http://mnras.oxfordjournals.org/ at INAF Trieste (Osservatorio Astronomico di Trieste) on January 8, 2016

grow via impulsive and exceptionally strong disc instabilities will inevitably, in these models, produce smaller bulges, preferentially in lower mass haloes, thus enhancing any environmental dependence.

Nevertheless, even in the absence of disc instabilities (right-hand panels), most models continue to predict a factor of ∼1.3–2 differences in the median sizes as a function of halo mass, which implies that other physical processes are contributing to environmental dependence. The G11 model shows an increase in median size by a cumulative factor of ∼1.4, and the MORGANA model with no disc instabilities predicts even more. The latter effect may be due to the fact that in the MORGANA model bulge growth via minor mergers is more efficient than in the G11 one, as in the former the whole baryonic mass of the satellite is transferred to the bulge of the central (Section 3). The S13 model also shows stronger environmental dependence with respect to the original G11 model, thus implying that the inclusion of gas dissipation and/or the null value of $f_{\rm orb}$ can contribute to this increase. We will further dissect the role played by different processes, by making use of the variations to the reference SHAM model introduced in Section 4.5.3.

4.5.2 A closer comparison to the data: including observational errors

As anticipated in Section 4.1, a proper comparison to the data requires convolution with observational errors. To achieve this goal, we follow the methodology outlined in Huertas-Company et al. (2013b). In each bin of halo mass, we randomly extract from the mocks a number of galaxies equal to the number actually extracted from the SDSS/Yang et al. catalogue. We then include errors in all the variables of interest following the methodology outlined in Section 4.1, recalibrate the slope β of the size–stellar mass relation, and finally recompute mass-dependent sizes following equation (16). We repeat the above process for 1000 times and for each mock realization compute median sizes. From the final distributions of medians we extract the final median value and its 1σ uncertainty. When dealing with galaxy populations in groups and cluster environments one should also consider field contamination, as we did in previous work (Huertas-Company et al. 2013b). However, we neglect the latter effect as we are here mainly interested in central galaxies.

We found that simply including only independent errors in all the three variables, namely size, stellar mass and halo mass, does not really alter the raw model predictions presented in the previous sections. This is mainly due to the fact that reasonable errors in stellar mass ($\gtrsim$ 0.2 dex) tend to preserve or even boost trends of median size with environment at fixed stellar mass. Lower mass and more compact galaxies preferentially residing in lower mass haloes, enter the selection creating a spurious increase of environmental dependence, or enhancing any pre-existing one (see simulations in Huertas-Company et al. 2013b).

More interesting to our purposes is instead the case of maximally correlated errors in size and stellar mass, and this is the one which will be discussed in this section. In the latter scenario, we found in fact that this combination of errors can produce an effective reduction of the environmental signal, thus providing a viable possibility to better reconcile model predictions with observational results. We checked that, as expected, fully correlated errors in size and stellar mass, while possibly relevant for environmental trends, do not significantly alter the slope β of the intrinsic size–stellar mass correlations, thus fully preserving the results discussed in Section 4.4. This is expected as varying size and stellar mass in a correlated way, tends to preferentially move galaxies along the relation. The total scatter, however, tends to somewhat increase up to about $\lesssim$30 per cent, irrespective of the exact model. We will discuss the relevance of this effect to our general discussion in Section 5.2.

The left-hand panels of Fig. 8 report the results of our Monte Carlo simulations including fully correlated errors in all the three variables. As for Fig. 7, the top panels report the median γ competing to galaxies within the chosen interval of stellar mass ($\log M_{\rm star}/{\rm M}_{\odot} > 11.2$), while the lower panels show the same curves normalized to the value in haloes $12.5 < \log M_{\rm halo}/{\rm M}_{\odot} < 13$. By comparing with the left-hand panels of Fig. 7, it can be seen that the inclusion of proper errors can alter the raw model outputs by significantly reducing the increase in median size with halo mass. In particular, we find that models predicting $\lesssim$30−40 per cent of environmental dependence (e.g. SHAM and G10), tend to be flattened out after inclusion of correlated errors. On the other hand, models with stronger environmental dependence at the level of $\gtrsim$50 per cent increase in median size when moving from field to clusters (e.g. S13 or MORGANA), tend to preserve significant size segregation. These findings are consistent with the results of the independent and different Monte Carlo tests performed by Huertas-Company et al. (2013b).

In the right-hand panels of Fig. 8 we show predictions for the same models as in the left-hand panels with errors in halo mass this time uncorrelated to the other quantities, following a Gaussian with dispersion of 0.3 dex (see Section 4.1). It is clear that in this case any trend with environment is further suppressed by up to an extra factor of $\lesssim$1.5, leaving at most a factor of $\lesssim$20 per cent at the highest halo masses. At variance with errors in stellar masses, substantial independent errors in halo mass tend to naturally further mix the host halo masses of galaxies at fixed stellar mass, thus contributing to reduce any signal with environment.

In conclusion, we showed that when including correlated errors, especially in size and stellar mass, we can alter model predictions and dump a significant part of the signal with environment. Estimating exact observational uncertainties, and correlations among them, becomes thus fundamental to break degeneracies in the models.

4.5.3 Varying the SHAM reference model

As evident from Figs 7 and 8, models characterized by having strong gas dissipation (S13) and/or stronger, impulsive bar instabilities (B06; MORGANA) produce the largest discrepancies with the data. To gain more insights into the causes of the discrepancies between hierarchical models and the data, we discuss in Fig. 9 the predictions of the different variations of the reference SHAM model introduced in Section 4.5.3, which bracket all the main physical processes discussed above.

Fig. 9 follows the same format as Figs 7 and 8, with the left-hand panels collecting the raw model predictions, while in the right-hand panels the predictions are convolved with fully correlated errors. Besides the reference SHAM (solid/orange lines), Fig. 9 contains predictions for other SHAM outputs, all characterized by $f_{\rm orb} = 0$, a choice which better matches the local size–mass relation (Section 4.4). The blue/dot–dashed lines refer to the SHAM which only varies $f_{\rm orb}$. The red/long-dashed lines refer to the SHAM which, in addition, also includes gas dissipation in major mergers. The magenta/triple dot–dashed lines correspond to the SHAM where satellites undergo quick quenching after infall. Finally, the black, thick, dotted lines refer instead to the SHAM run with reduced dynamical friction time-scales.

Downloaded from http://mnras.oxfordjournals.org/ at INAF Trieste (Osservatorio Astronomico di Trieste) on January 8, 2016

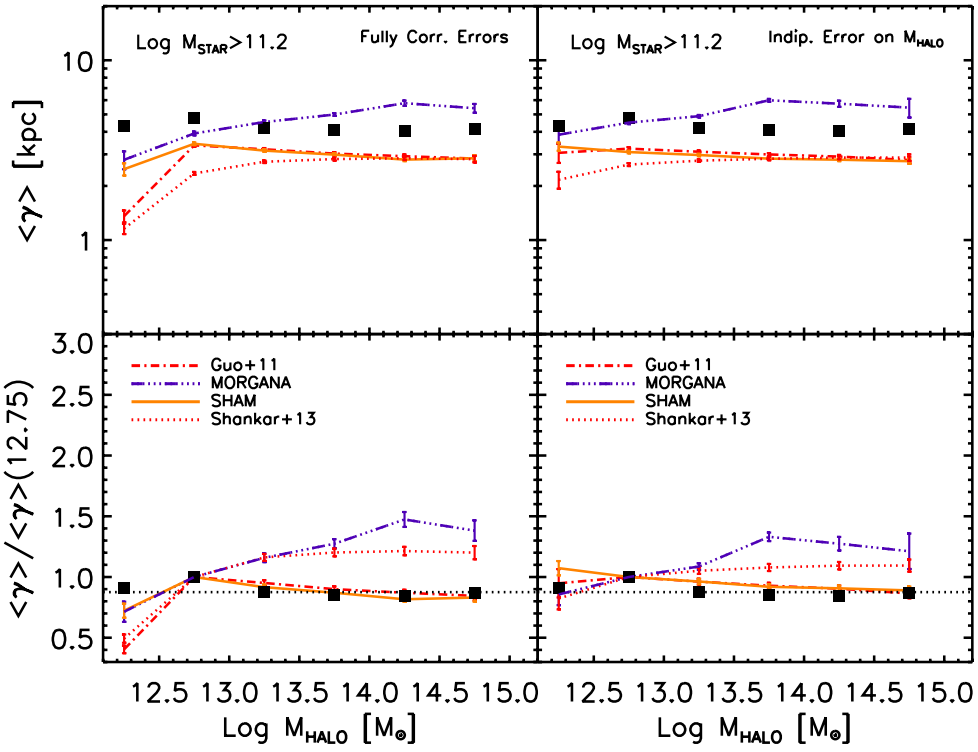

Figure 8. Top: predicted median γ sizes for the same set of models as in Fig. 7, as labelled. Bottom: corresponding fractional increase of median size. In the left-hand panels all predictions are convolved with fully correlated errors, while in the right-hand panels we assume errors in halo mass to be independent (see the text for details). Models with strong gas dissipation in major mergers, and/or very low dynamical friction time-scales are disfavoured, although the effect is weakened in the presence of specific combinations of correlated errors.

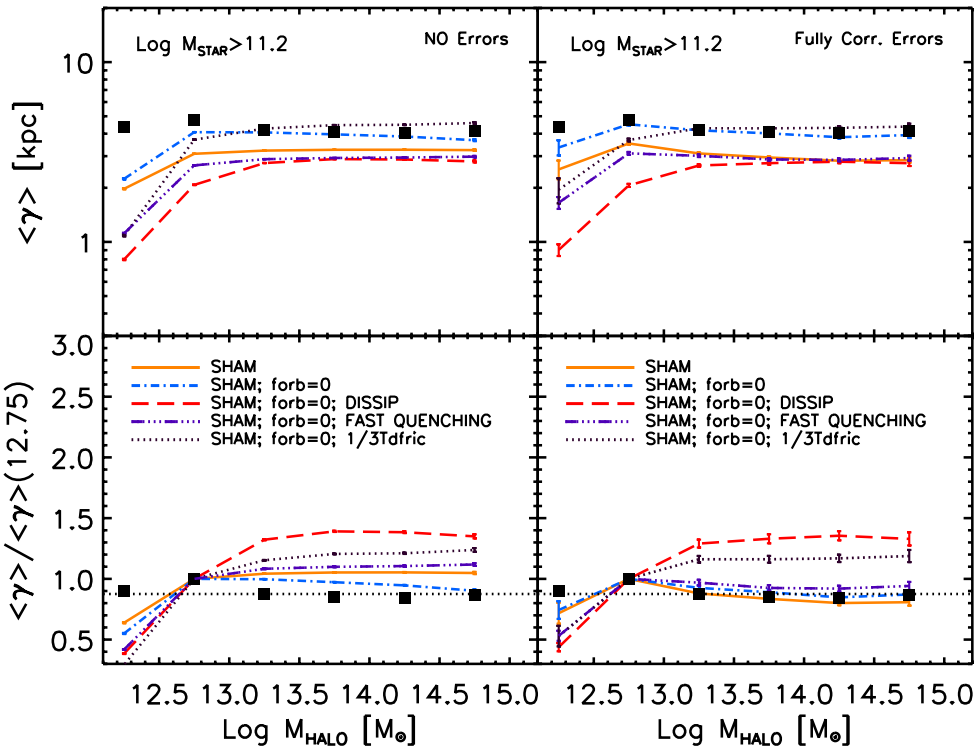

Figure 9. Same format as Fig. 7 for different SHAM models, as labelled. The left-hand panels report raw predictions, the right-hand panels present models predictions after convolution with errors. Even in the semi-empirical formalism, models with strong gas dissipation in major mergers, and/or very low dynamical friction time-scales, tend to be disfavoured.

Downloaded from http://mnras.oxfordjournals.org/ at INAF Trieste (Osservatorio Astronomico di Trieste) on January 8, 2016

Table 2. List of main physical processes identified in this work which can cause environmental dependence in the median size of central, bulge-dominated early-type galaxies at fixed stellar mass. The second column briefly provides the main features characterizing each process within the context of environment. The third column details if the signal with environment, specifically induced by a given process, is still detectable after inclusion of systematic and statistical errors in size, stellar mass and host halo mass, following the discussion in Section 4.5.2.

Process	Description	After errors
Disc instabilities	Mostly effective if violent and impulsive. Induce more compact bulges in less massive haloes with lower circular velocities.	Only marginally reduced
Mergers	Only effective (at $z = 0$) if short dynamical friction time-scales. More effective (minor) galaxy mergers in more massive host haloes, thus larger centrals.	Only marginally reduced
Gas dissipation	Progressively more effective in less massive haloes with gas richer progenitors.	Only marginally reduced
Satellite evolution	Overall milder effect. Present if fast quenching/gas stripping, thus proportionally less growth in satellites in lower mass haloes. Induces more compact remnants in less massive haloes.	Significantly reduced

It can be seen that models characterized by lower dynamical friction time-scales, and/or strong gas dissipation in major mergers, and/or fast quenching, tend to increase any environmental dependence, with the gas dissipation model predicting the strongest steepening with halo mass, in line with the S13 model. As more extensively discussed below, gas dissipation in major mergers tends to decrease the sizes of the remnants, progressively more efficiently in lower mass haloes. This is because the satellite progenitors in these environments tend to be relatively gas richer thus inducing more dissipation and more compact remnants.

Just the opposite is true when lowering the merging time-scale. In the latter case lowering $t_{\rm df}$ increases the number of mergers with the central galaxy especially in more massive haloes, boosting their size increase. Note also that faster mergers also imply less growth time via star formation for satellites in intermediate to low-mass haloes, thus proportionally decreasing the sizes of the final remnants. This is the main reason why galaxies in haloes with $\log M_{\rm halo}/{\rm M}_{\odot} \lesssim 13$ tend to be smaller than galaxies of similar stellar mass in the model with longer $t_{\rm df}$ (see also Fig. 4). The combination of these two effects produces a steeper correlation of median sizes with respect to host halo masses (dotted lines) than the same model with longer dynamical time-scales (dot–dashed lines).

From Fig. 9 it also appears that the final sizes in the fast quenching model (triple dot–dashed lines) are more compact with respect to a model with delayed quenching (dot–dashed lines), and the effect is more relevant in lower mass host haloes. This result can be understood in our framework by recalling that a faster quenching implies smaller and less massive satellites and a proportionally more contained growth for centrals. Given that the SSFR has a strong inverse dependence with stellar mass (equation 12), lower mass galaxies grow proportionally more than more massive ones within the same interval of time. Thus, a faster quenching will more severely limit the growth of the lowest massive galaxies, the latter being preferentially satellites in lower mass haloes. We thus expect a faster satellite quenching to have, on average, a relatively more pronounced effect for the growth of centrals in lower mass haloes.

5 DISCUSSION

5.1 The physics behind environmental dependence

We have so far identified several physical effects which can cause a variation in the median size of bulge-dominated central galaxies of similar stellar mass when moving from lower to higher mass host haloes. Table 2 contains a list of these processes, providing a brief description for each one of them within the context of environment, and specifying if the signal with environment, specifically induced by a given process, is still detectable after inclusion of systematic and statistical errors in size, stellar mass and host halo mass, following the discussion in Section 4.5.2.

We can summarize the physical processes identified in the previous sections as follows.

(i) *Disc instabilities*. We discussed in reference to Fig. 7, that models characterized by strong and impulsive disc instabilities tend to grow massive bulges in less massive haloes. The instability criteria usually adopted in SAMs in fact (e.g. equation 4), are more easily met by massive galaxies in lower mass haloes, at fixed stellar mass. Being instabilities less efficient than mergers in building large bulges of same stellar mass (cf. equation 5), this naturally increases the halo mass dependence in median sizes. Models characterized by strong disc instabilities can predict an increase in size of a factor of $\gtrsim$2 when moving from field to clusters, difficult to reconcile with the data, even after convolution with substantial observational errors. We here stress, however, that violent disc instabilities, especially in high-redshift, clumpy star-forming discs could still play a substantial role in building stellar bulges (e.g. Dekel, Sari & Ceverino 2009; Bournaud et al. 2011a,b). If, for example, violent disc instabilities are more common than previously thought (e.g. Bournaud et al. 2013; Mandelker et al. 2013), then they can be triggered in different environments, thus reducing the tension with the data. What our findings seem to suggest is that the usually adopted analytic modelling for these types of processes (Section 3), may still not be entirely appropriate for describing the complexities characterizing the different stages and modes of disc instabilities (e.g. Athanassoula, Machado & Rodionov 2013).

Downloaded from http://mnras.oxfordjournals.org/ at INAF Trieste (Osservatorio Astronomico di Trieste) on January 8, 2016

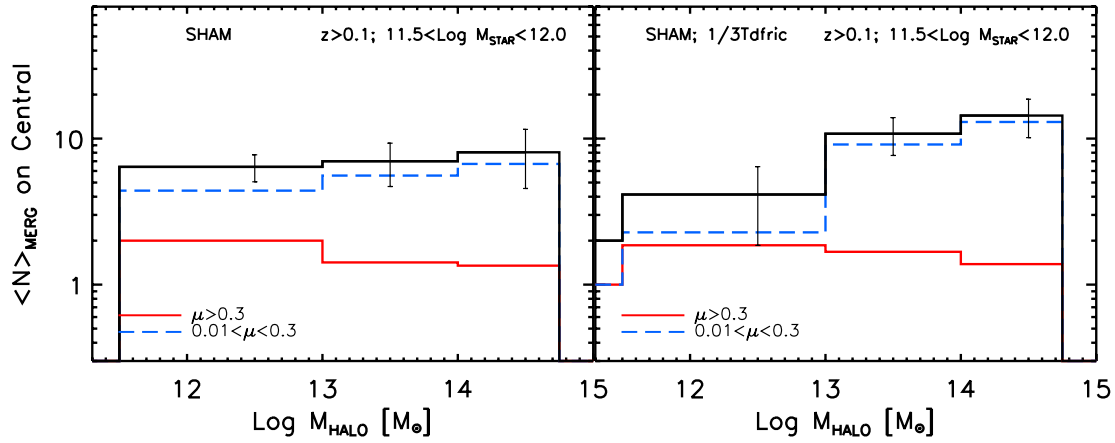

Figure 10. Predicted cumulative mean number of mergers on the central galaxy as a function of host halo mass at $z = 0$. Marked with blue, long-dashed and red, solid lines are the cumulative number of minor and major mergers down to $z = 0$, respectively, with the black, solid lines the sum of the two. The vertical bars indicate the 1σ uncertainties on the total number of mergers in each bin of halo mass. The left-hand panel shows the reference SHAM model with dynamical friction time-scales $t_{\rm df}$ from McCavana et al. (2012), while the right-hand panel reports the outputs of a model with 1/3 of the same merger time-scales. Overall, it is evident that adopting the dynamical friction time-scales expected from the analysis of high-resolution numerical simulations (left), the number of mergers at fixed stellar mass does not significantly increase with halo mass. Here the analysis is restricted to galaxies with stellar masses $11.5 < \log M_{\rm star}/{\rm M}_{\odot} < 12$ and $B/T > 0.5$, but the basic result of a flattish distribution of mergers is similar for other selections. On the other hand, shorter dynamical friction time-scales inevitably increase the number of (minor) mergers in more massive haloes, thus inducing more size growth and more environmental dependence.

(ii) *Mergers/dynamical friction time-scales*. We showed that even in the absence of strong disc instabilities, hierarchical models may still produce significant environmental dependence. This is particularly true for models with efficient merging, either induced by more bulge growth (MORGANA) and/or lower dynamical friction time-scales (B06, SHAM-low $t_{\rm df}$). For models with relatively longer $t_{\rm df}$ (G11, SHAM), environmental dependence is minimal. This is mainly induced by the fact that, owing to the self-similarity of dark matter, the number of cumulative mergers down to $z = 0$ on the central galaxy at fixed interval of stellar mass, does not largely increase when moving from low- to high-mass host haloes, with a moderate variation of up to a factor of $\lesssim$1.3–1.5. This is clearly seen in Fig. 10, which plots the average total number of mergers for galaxies of stellar mass $11.5 < \log M_{\rm star}/{\rm M}_{\odot} < 12$ as a function of host halo mass down to $z = 0$. The left-hand panel plots the expectations of our reference SHAM based on $t_{\rm df}$ taken from the recent high-resolution simulations by McCavana et al. (2012), while the right-hand ones of the SHAM run with the same dynamical friction time-scales shortened by a factor of 1/3. Central galaxies in more massive haloes have a tendency to have on average more minor mergers, while the number of major mergers, is roughly comparable in all environments (see also, e.g. Hirschmann et al. 2013). This implies that centrals in more massive haloes will have a tendency for being larger. However, this size increase must also be relatively modest, as the cumulative number of mergers in the most massive haloes is at the most a factor of $\lesssim$1.3 higher than in less massive haloes. On the other hand, the number of *minor* (but not major) mergers increases by up to a factor of $\sim$4 for the model characterized by lower $t_{\rm df}$. If the merger time-scales are sufficiently short, then galaxies at the centres of clusters will tend to undergo more effective galaxy merging, thus naturally increasing their sizes and boosting any environmental dependence. Interestingly, lower dynamical friction time-scales were favoured by, e.g. Newman et al. (2012) to speed up the size growth of massive galaxies and improve the match with the data. We note that although merging may not be the dominant cause of environmental dependence at $z = 0$, this does not exclude that it may still induce a stronger environmental trend at higher redshifts. In fact, early-type galaxies born in denser environments are expected to undergo a boosted evolution at $z > 1$, thus forming larger bulges at these epochs, in line with the observational evidence briefly summarized in Section 1 (e.g. Delaye et al. 2013). We will further investigate the full evolution of bulge-dominated galaxies in different environments and their impact on size evolution in subsequent work (Shankar et al., in preparation).

(iii) *Gas dissipation in (major) mergers*. Taken at face value, gas dissipation can produce a factor of $\sim$2 increase in median size when moving from field to cluster environments, in apparent disagreement with the data (Figs 7 and 9). Within a given stellar mass bin, it is naturally expected that gas dissipation will more effectively shrink the sizes of the lowest mass and gas richer galaxies (equation 3). This in turn will induce environmental dependence, given that lower mass galaxies preferentially live in lower mass haloes. However, even at fixed stellar mass galaxies residing in lower mass haloes will continue to have a higher probability to merge with massive, gas richer satellites. This is because lower mass host haloes are more easily invested by lower stellar mass satellites with sufficiently high gas content to overcome the baryonic threshold for triggering a (dissipative) major merger (see Section 3). To better visualize the latter effect, in Fig. 11 we report the median total gas content of progenitors extracted from the SHAM model. We consider the gas fractions in the pre-merger phase as a function of host halo mass, weighted in a way to minimize any additional spurious trend due to the stellar mass dependence in the input gas fractions (equation 9). We first compute the quantity

$$F_{\rm gas,merg} = M_{\rm gas,prog}/(M_{\rm star,prog} + M_{\rm star,burst}), \quad (17)$$

which is the ratio between total gas content of progenitors in major mergers, and the sum of the total stellar mass of the progenitors plus the amount of mass formed during the merger (computed via equation 6). The latter quantity is just the fraction used in equation (3). The higher the gas fraction $F_{\rm gas,\,merg}$, the more compact the remnant will be. To then make a proper comparison among progenitors of different mass, similarly to what we do for sizes we weight $F_{\rm gas,\,merg}$ with respect to the remnant's stellar mass as

$$\log F_{\rm gas,prog} = \log F_{\rm gas,merg} + \alpha(z)[11 - \log M_{\rm star}], \quad (18)$$

Downloaded from http://mnras.oxfordjournals.org/ at INAF Trieste (Osservatorio Astronomico di Trieste) on January 8, 2016

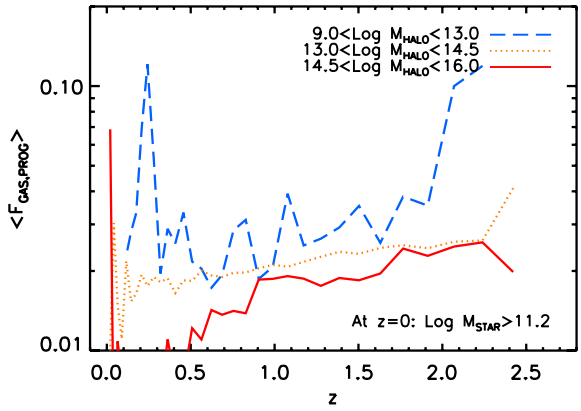

Figure 11. Predicted redshift evolution along the main branch of the median gas content in the progenitors before a major merger for galaxies with $\log M_{\rm star}/{\rm M}_{\odot} > 11.2$ at $z = 0$, living at the centre of different host halo masses, as labelled. Massive galaxies in lower mass haloes tend to always be gas richer because the progenitors are less massive and thus gas richer.

with $\alpha(z)$ being the same as in equation (9). The result is reported in Fig. 11, which shows that the progenitors of centrals in less massive haloes are always gas richer. This in turn explains why the remnants are proportionally more compact, as gas dissipation produces more compact remnants, the gas richer merging progenitors (equation 3). The non-ideal performance of models with gas dissipation is particularly intriguing. The latter process has been recognized to play a significant role in hydrosimulations (Hopkins et al. 2009; Covington et al. 2011), and also to help in better reproducing other scaling relations, such as the ones with age and velocity dispersion (Shankar et al. 2013), or possibly also between bulge size and stellar mass, as discussed in Section 4.4. On the other hand, as mentioned in Section 4.4, a properly fine-tuned disc regrowth/survival mechanism may suitably increase the total sizes of remnants in gas richer environments, thus helping to better match the R_e–$M_{\rm star}$ relation (Fig. 4), and at the same time reduce environmental dependence. We will explore such possibilities in future work.

(iv) *Evolution of satellites*: gas consumption, quenching and stripping. Including quenching in the model implies restricting the growth of infalling satellites. In turn, fast quenching tends to produce more compact remnants at fixed stellar mass with respect to the data, although the difference could still be within the 1σ uncertainty (cf. Fig. 5). More interestingly, we pointed out with respect to Fig. 9, that a model with fast quenching predicts some enhanced environmental size dependence with respect to a model with slower quenching. As shown in Section 4.5.3, the latter effect can be broadly understood along the following lines. In general, galaxies of a given stellar mass residing in less massive haloes, will preferentially merge with lower mass, gas richer and more star-forming satellites, the latter two features being a direct consequence of the anticorrelation between gas fractions and SSFR with stellar mass (equations 9 and 12, respectively). In other words, within the same amount of time, lower mass satellites grow proportionally more than more massive ones. In a fast quenching scenario, however, satellites' growth is inhibited, proportionally more in lower mass haloes invested by the least massive satellites. Centrals in lower mass haloes are thus expected to grow less in size with respect to their counterparts in more massive haloes. Indeed, we have verified that the number of (minor) mergers (down to 1 per cent in progenitors' mass ratio) is reduced by $\sim(30 \pm 20)$ per cent for centrals in haloes $\log M_{\rm halo}/{\rm M}_{\odot} \lesssim 13$ with respect to the reference model in the left-hand panel of Fig. 10, thus proportionally preventing their size growth. The fast quenching process, however, tends to be weaker than the previous ones in the list, since the difference in number of mergers between less and more massive haloes is less than 1.5σ. The net effect is nevertheless visible in the top left-hand panel of Fig. 9, where central galaxies in haloes below $\log M_{\rm halo}/{\rm M}_{\odot} \lesssim 13$ appear progressively more compact in the fast quenching model (triple dot–dashed line) than in the slower quenching one (solid line). Finally, as discussed in Appendix A, a model with faster quenching will tend to retain larger fractions of gas with respect to what actually observed, at least at this basic level of the modelling.

5.2 Scatter around the $R_e - M_{\rm star}$ relation

So far we mainly focused on the slopes of the size–stellar mass relations and discussed dispersions around this relation only in terms of dependence on host halo mass. We here discuss model predictions in terms of *total* scatter around the median. We should immediately emphasize that studying total scatter around the median size–stellar mass relation, i.e. its global 1σ dispersion, although possibly correlated, is not necessarily equivalent to study environmental dependence as we did in the previous sections. In fact, until now our concern was focused on probing departures from the median of specific subclasses of galaxies, labelled by different host halo masses. Such deviations were further weighted to take into account the exact location of each galaxy on the relation, irrespective of how large the bin in stellar mass is considered. This methodology can thus easily produce dispersions different from the canonical 1σ, rigourously computed for all galaxies in a narrow bin of stellar mass. For example, Shankar et al. (2013) showed that the G11 model with or without dissipation produces very similar global dispersions around the mean relation, especially for the most massive galaxies (their fig. 5), despite the inclusion of dissipation inducing an environmental dependence systematically higher by a factor of $\gtrsim$1.5 (Fig. 7). As an additional proof, we have also checked that all the results on the total scatter presented below do not change significantly if, for example, we exclude from the analysis massive groups and clusters. Limiting the sample to haloes less massive than, say, $M_{\rm halo} \lesssim 3 \times 10^{13}\,{\rm M}_{\odot}$, yields in fact nearly identical results, except for entirely cutting out galaxies in the highest bins of stellar mass, as expected. We will thus proceed discussing the results on global scatter mostly as a separate issue with respect to environmental dependence, although we will highlight connections where relevant.

Fig. 12 compares the outcomes of our reference hierarchical galaxy models with respect to the data (solid/black line). We confirm previous claims (e.g. Nair et al. 2011; Bernardi et al. 2013) for an extremely tight correlation in the observed relation with $\Delta \ln R_e \sim 0.35$, i.e. just $\sim$0.15 dex. Bernardi et al. (2013) have recently showed via Monte Carlo simulations that the intrinsic, true scatter should in fact be even smaller by a factor of $\gtrsim$1.5−2 (cf. their fig. 13).

All hierarchical models instead tend to predict much larger dispersions than those observed. Here we only focus on the raw predictions of the models but, as anticipated in Section 4.5.2, any convolution with correlated and statistical errors would enhance the predicted scatter by up to $\sim$30 per cent, clearly worsening the comparison to the data. The causes behind such broadening are multiple. First, disc instabilities can effectively increase the scatter in the scaling relations involving sizes. If modelled as in equation (5), disc instabilities will always be less efficient than mergers in building large bulges,

Downloaded from http://mnras.oxfordjournals.org/ at INAF Trieste (Osservatorio Astronomico di Trieste) on January 8, 2016

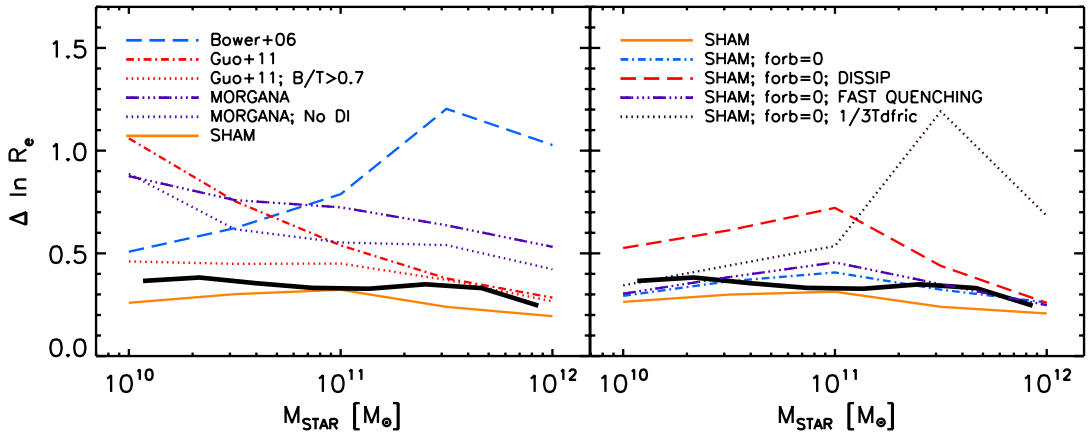

Figure 12. Predicted scatter around the median size–stellar mass relation for different models (left), and for different variations within the SHAM (right). Data are extracted from the Huertas-Company et al. (2013b) catalogue. Most models predict a large scatter. However, a large fraction of this scatter is caused by galaxies with lower B/T. Bulge-dominated galaxies, with $B/T > 0.7$, tend to better line up with the data. SHAMs, characterized by having tighter relations in the scaling relations of progenitors, tend to provide a better match to the data (see the text for details).

irrespective of the type of disc instability considered, either moderate ones as in G11, or stronger ones as in B06. Thus, similarly to what discussed in reference to environmental dependence, at fixed stellar mass disc instabilities will also generate a larger fraction of more compact bulges, increasing the scatter. The left-hand panel of Fig. 12 shows that the large size distribution in the G11 model (dot–dashed, red line) for stellar masses below $M_{\rm star} \lesssim 10^{11}\,{\rm M}_{\odot}$, is mainly caused by stellar bar instabilities. In line with what highlighted by Shankar et al. (2013), a large fraction of bulges in this mass range is built via secular processes. Restricting instead to bulge-dominated galaxies with $B/T > 0.7$ (red, dotted line), with mostly merger-driven growth (Shankar et al. 2013), neatly cuts out all outliers beyond $\Delta\ln R_e \gtrsim 0.5$. Similarly, the MORGANA model (triple dot–dashed, purple line) also predicts a large scatter, which is significantly reduced to $\Delta\ln R_e \lesssim 0.6$ for massive galaxies if disc instabilities are not included (dotted, purple line). The B06 model predicts large dispersions with respect to the data, at all stellar masses. We believe that at least part of this discrepancy is due to the strong disc instabilities and the relatively lower dynamical friction time-scales included in this model (see Section 3.1).

Even after removing disc instabilities, models still tend to predict larger scatters than observed. This is clear from the left-hand panel of Fig. 12 as both the MORGANA and the G11 models (purple and red dotted lines, respectively) still lie above the data at all stellar masses. It was already pointed out that the chaotic nature of galaxy merger trees could in fact generate too large size distributions at fixed stellar mass with respect to what actually measured in the local Universe (e.g. Nipoti et al. 2009; Nair et al. 2011; Shankar et al. 2013). However, the disagreement with the data although significant, is not large. Indeed, we find that the SHAM, despite being built in a very similar hierarchical context as for the other models, predicts an exceptionally limited dispersion, actually somewhat lower than the observed one, and possibly comparable to the intrinsic one claimed by Bernardi et al. (2013). We checked in fact that, at least above $\log M_{\rm star}/{\rm M}_{\odot} \gtrsim 11.2$, the predicted scatter from the SHAM inclusive of all errors amounts to $\Delta\ln R_e \sim 0.3$, in close agreement to the observed one. The success of the latter model relies on the very tight input scaling relations in mass and size defining the progenitor disc galaxies. For example, as detailed in Section 3.4, in our reference model we have assumed discs to follow an empirical, time-dependent disc size–stellar mass relation, with an intrinsic Gaussian scatter of 0.1 dex. We checked that increasing this scatter, proportionally boosts the final dispersion around the size–stellar mass relation of the remnant bulge-dominated galaxies. In other words, galaxy merger trees may not necessarily broaden the input correlations. A similar conclusion has been recently reached by Taranu, Dubinski & Yee (2013), who demonstrated via collisionless simulations of dry mergers in group environments, that stochastic merging can indeed produce tight scaling relations for early-type remnants, as long as the merging galaxies also follow tight scaling relations.

We find the latter conclusion to be quite robust against variations in the input assumptions of the SHAM model. By varying orbital energies ($f_{\rm orb}$), or the time for quenching, only mildly impacts the resulting scatter in sizes (dot–dashed, blue and triple dot–dashed, purple lines, respectively). The only notable exceptions are variations in $t_{\rm df}$ and, possibly, gas dissipation. Despite the short $t_{\rm df}$ model (dotted, black line, right-hand panel) being identical to the reference SHAM (i.e. very tight scaling relations for the progenitors), the resulting correlations for bulges appear quite broader, especially at masses above $\gtrsim 10^{11}\,{\rm M}_{\odot}$, which are the ones most affected by mergers. Indeed, when mergers become too numerous they can induce chaotic behaviours in the resulting scaling relations, in line with previous claims. However, when proper (sufficiently long) $t_{\rm df}$ are adopted, alongside with tight scaling relations for progenitors, then mergers can preserve tight scaling relations for remnants.

The SHAM model with gas dissipation (red, long-dashed line, right-hand panel) tends to produce a scatter larger than the ones without dissipation around $M_{\rm star} \lesssim 2 \times 10^{11}\,{\rm M}_{\odot}$, but comparable at increasingly higher stellar masses, broadly in line with what was claimed by Shankar et al. (2013). We can partly ascribe the increase in dispersion at intermediate and lower stellar masses to the slow quenching time-scales assumed in the reference SHAM. We checked in fact that by increasing the quenching and/or the stripping would better limit the growth of the scatter in sizes, especially in the model with dissipation.

Overall, what is most relevant to the present discussion is that mergers alone do not necessarily imply larger scatters in size distributions with respect to what was observed. As long as the dynamical time-scales are sufficiently long, comparable to what was suggested by detailed N-body simulations, and the scaling relations of progenitors are sufficiently tight, the complex mixture of mergers may still preserve a contained scatter in the remnants, closer to what is observed.

Downloaded from http://mnras.oxfordjournals.org/ at INAF Trieste (Osservatorio Astronomico di Trieste) on January 8, 2016

6 CONCLUSIONS

In this work we have compared state-of-the-art SAMs of galaxy formation as well as advanced SHAM, with a large sample of early-type galaxies from SDSS. In particular, we focused our attention on the environmental dependence of sizes of central galaxies as a function of host halo mass. In the data, information on host halo mass is derived by cross-correlating the SDSS morphological sample by Huertas-Company et al. (2013a) with the Yang et al. (2007) halo catalogue. Sizes are derived from Sérsic fits to the SDSS images (Bernardi et al. 2013). We then selected early-type galaxies with $\log M_{\rm star}/{\rm M}_{\odot} > 11.2$. We find a flat distribution of median size as a function of host halo mass, in line with previous studies in the local Universe (e.g. Guo et al. 2009; Huertas-Company et al. 2013b).

All hierarchical models considered in this work instead tend to predict a moderate to strong environmental dependence, with the median size difference of a factor of $\sim$1.5–3 when moving from the lowest ($\gtrsim 3 \times 10^{12}\,{\rm M}_{\odot}$) to the highest ($\sim 10^{15}\,{\rm M}_{\odot}$) host halo masses. At face value the discrepancy with the data is highly significant. However, the convolution with the (correlated) errors in the observations, can wash out part of the trends with host halo mass predicted by some models, thus lowering the significance of the discrepancy. We however find that those models which predict a difference higher than a factor of $\gtrsim$1.5–2, tend to preserve the signal in samples with the same number of galaxies as in SDSS.

Despite the observational uncertainties, the data tend to disfavour hierarchical models characterized by strong and impulsive disc instabilities, strong gas dissipation in major mergers, short dynamical friction time-scales, and very short quenching time-scales in infalling satellites. These results hold irrespective of the model adopted, semi-analytic or semi-empirical. Interestingly, mergers at the rate predicted by *N*-body simulations are not a major cause for environmental dependence in the local Universe, because the cumulative number of mergers on the central galaxies down to $z = 0$, and thus their related size growth, is not a strong function of host halo mass at fixed bin of stellar mass.

Galaxies residing in less massive haloes are preferentially involved in mergers with gas richer satellites, thus inducing proportionally more gas dissipation, more compact remnants and more environmental dependence. Also, galaxies residing in less massive haloes more frequently meet the condition for disc instabilities (massive discs in relatively less massive haloes), triggering the growth of bulges with smaller sizes with respect to equally massive bulges grown via mergers, thus further increasing any environmental dependence. Finally, if the quenching of satellites is sufficiently rapid, then this will impact more efficiently less massive galaxies with the highest SSFRs. In turn, central galaxies residing in less massive haloes, involved preferentially in minor mergers with the least massive satellites, will grow proportionally less in size than their counterparts in more massive haloes, thus inducing additional environmental dependence. We discuss possibilities to alleviate tensions between models and the data in Section 5.

We also discussed additional key issues related to sizes and environment in bulge-dominated galaxies and to the hierarchical models considered above. Most importantly, we showed that the size–stellar mass relation of local galaxies can be well reproduced by hierarchical models both in slope and scatter as long as the scaling relations of the disc progenitors are sufficiently tight, and the dynamical friction time-scales are sufficiently long.

It will be interesting to discuss detailed model predictions to higher redshifts where, as referenced in Section 1, there is now growing evidence for an accelerated structural evolution of massive galaxies in denser environments. In fact merging could still induce a faster evolution of galaxies in very dense regions, which could create an apparent trend with environment at high redshifts. We leave the exploration of these issues to separate work (Shankar et al., in preparation).

Environment continues to play a significant role in constraining galaxy evolution. When future dynamical and spectral observations of massive, early-type galaxies and their surroundings will be able to further tighten the measurements on size, stellar mass and halo mass, the constraints will become invaluable to discern among the successful galaxy formation models.

ACKNOWLEDGEMENTS

FS warmly thanks Simona Gattorno for all her kind and continuous support. FS acknowledges support from a Marie Curie Grant. FF acknowledges financial support from the Klaus Tschira Foundation and the Deutsche Forschungsgemeinschaft through Transregio 33, 'The Dark Universe'. We thank an anonymous referee for a constructive report that helped improving the presentation of the results.

REFERENCES

Abazajian K. N. et al., 2009, ApJS, 182, 543
Aguerri J. A. L., Sánchez-Janssen R., Muñoz-Tuñón C., 2007, A&A, 471, 17
Angulo R. E., Lacey C. G., Baugh C. M., Frenk C. S., 2009, MNRAS, 399, 983
Athanassoula E., Machado R. E. G., Rodionov S. A., 2013, MNRAS, 429, 1949
Bakos J., Trujillo I., 2012, preprint (arXiv:1204.3082)
Bassett R. et al., 2013, ApJ, 770, 58
Behroozi P. S., Conroy C., Wechsler R. H., 2010, ApJ, 717, 379
Bernardi M., 2009, MNRAS, 395, 1491
Bernardi M. et al., 2003, AJ, 125, 1817
Bernardi M., Shankar F., Hyde J. B., Mei S., Marulli F., Sheth R. K., 2010, MNRAS, 404, 2087
Bernardi M., Roche N., Shankar F., Sheth R. K., 2011a, MNRAS, 412, L6
Bernardi M., Roche N., Shankar F., Sheth R. K., 2011b, MNRAS, 412, 684
Bernardi M., Meert A., Vikram V., Huertas-Company M., Mei S., Shankar F., Sheth R. K., 2012, preprint (arXiv:1211.6122)
Bernardi M., Meert A., Sheth R. K., Vikram V., Huertas-Company M., Mei S., Shankar F., 2013, MNRAS, 436, 697
Bournaud F. et al., 2011a, ApJ, 730, 4
Bournaud F., Dekel A., Teyssier R., Cacciato M., Daddi E., Juneau S., Shankar F., 2011b, ApJ, 741, L33
Bournaud F. et al., 2013, ApJ, 780, 57
Bower R. G., Benson A. J., Malbon R., Helly J. C., Frenk C. S., Baugh C. M., Cole S., Lacey C. G., 2006, MNRAS, 370, 645 (B06)
Boylan-Kolchin M., Ma C.-P., Quataert E., 2008, MNRAS, 383, 93
Bruzual G., Charlot S., 2003, MNRAS, 344, 1000
Carollo C. M. et al., 2013, ApJ, 773, 112
Catinella B. et al., 2010, MNRAS, 403, 683
Cattaneo A., Mamon G. A., Warnick K., Knebe A., 2011, A&A, 533, A5
Chabrier G., 2003, PASP, 115, 763
Chiosi C., Merlin E., Piovan L., 2012, preprint (arXiv:1206.2532)
Cimatti A., Nipoti C., Cassata P., 2012, MNRAS, 422, L62
Cole S., Lacey C. G., Baugh C. M., Frenk C. S., 2000, MNRAS, 319, 168
Cooper M. C. et al., 2012, MNRAS, 419, 3018
Covington M. D., Primack J. R., Porter L. A., Croton D. J., Somerville R. S., Dekel A., 2011, MNRAS, 415, 3135
De Lucia G., Blaizot J., 2007, MNRAS, 375, 2
De Lucia G., Springel V., White S. D. M., Croton D., Kauffmann G., 2006, MNRAS, 366, 499

Downloaded from http://mnras.oxfordjournals.org/ at INAF Trieste (Osservatorio Astronomico di Trieste) on January 8, 2016

De Lucia G., Boylan-Kolchin M., Benson A. J., Fontanot F., Monaco P., 2010, MNRAS, 406, 1533
De Lucia G., Fontanot F., Wilman D., Monaco P., 2011, MNRAS, 414, 1439
de Vaucouleurs G., 1948, Ann. Astrophys., 11, 247
Dekel A., Sari R., Ceverino D., 2009, ApJ, 703, 785
Delaye L. et al., 2013, preprint (arXiv:1307.0003)
Efstathiou G., Lake G., Negroponte J., 1982, MNRAS, 199, 1069
Fan L., Lapi A., Bressan A., Bernardi M., De Zotti G., Danese L., 2010, ApJ, 718, 1460
Fontanot F., De Lucia G., Wilman D., Monaco P., 2011, MNRAS, 416, 409
Fu J., Guo Q., Kauffmann G., Krumholz M. R., 2010, MNRAS, 409, 515
Fu J. et al., 2013, MNRAS, 434, 1531
González J. E., Lacey C. G., Baugh C. M., Frenk C. S., Benson A. J., 2009, MNRAS, 397, 1254
Guo Y. et al., 2009, MNRAS, 398, 1129
Guo Q., White S., Li C., Boylan-Kolchin M., 2010, MNRAS, 404, 1111
Guo Q. et al., 2011, MNRAS, 413, 101 (G11)
Guo Q., White S., Angulo R. E., Henriques B., Lemson G., Boylan-Kolchin M., Thomas P., Short C., 2013, MNRAS, 428, 1351
Harker G., Cole S., Helly J., Frenk C., Jenkins A., 2006, MNRAS, 367, 1039
Henriques B. M. B., White S. D. M., Lemson G., Thomas P. A., Guo Q., Marleau G.-D., Overzier R. A., 2012, MNRAS, 421, 2904
Hirschmann M., De Lucia G., Iovino A., Cucciati O., 2013, MNRAS, 433, 1479
Hopkins P. F., Hernquist L., Cox T. J., Keres D., Wuyts S., 2009, ApJ, 691, 1424
Hopkins P. F. et al., 2010, ApJ, 724, 915
Huertas-Company M., Aguerri J. A. L., Bernardi M., Mei S., Sánchez Almeida J., 2011, A&A, 525, A157
Huertas-Company M. et al., 2013a, MNRAS, 428, 1715
Huertas-Company M., Shankar F., Mei S., Bernardi M., Aguerri J. A. L., Meert A., Vikram V., 2013b, ApJ, 779, 29
Ishibashi W., Fabian A. C., Canning R. E. A., 2013, MNRAS, 431, 2350
Karim A. et al., 2011, ApJ, 730, 61
Karim A. et al., 2013, MNRAS, 432, 2
Kauffmann G. et al., 2012, MNRAS, 422, 997
Khochfar S., Burkert A., 2006, A&A, 445, 403
Khochfar S. et al., 2011, MNRAS, 417, 845
Krause E., Hirata C. M., Martin C., Neill J. D., Wyder T. K., 2013, MNRAS, 428, 2548
Kravtsov A. V., 2013, ApJ, 764, L31
Lani C. et al., 2013, MNRAS, 435, 207
Leauthaud A. et al., 2010, ApJ, 709, 97
McCavana T., Micic M., Lewis G. F., Sinha M., Sharma S., Holley-Bockelmann K., Bland-Hawthorn J., 2012, MNRAS, 424, 361
Maltby D. et al., 2010, MNRAS, 402, 282
Mandelker N., Dekel A., Ceverino D., Tweed D., Moody C. E., Primack J., 2013, preprint (arXiv:1311.0013)
Meert A., Vikram V., Bernardi M., 2013, MNRAS, 433, 1344
Mei S. et al., 2012, ApJ, 754, 141
Mendel J. T., Simard L., Ellison S. L., Patton D. R., 2013, MNRAS, 429, 2212
Mo H. J., Mao S., White S. D. M., 1998, MNRAS, 295, 319
Mok A. et al., 2013, MNRAS, 431, 1090
Monaco P., Theuns T., Taffoni G., 2002, MNRAS, 331, 587
Monaco P., Murante G., Borgani S., Fontanot F., 2006, ApJ, 652, L89
Moster B. P., Naab T., White S. D. M., 2013, MNRAS, 428, 3121
Muzzin A. et al., 2012, ApJ, 746, 188
Naab T., Johansson P. H., Ostriker J. P., 2009, ApJ, 699, L178
Nair P., van den Bergh S., Abraham R. G., 2011, ApJ, 734, L31
Neistein E., Li C., Khochfar S., Weinmann S. M., Shankar F., Boylan-Kolchin M., 2011, MNRAS, 416, 1486
Newman A. B., Ellis R. S., Bundy K., Treu T., 2012, ApJ, 746, 162
Newman A. B., Ellis R. S., Andreon S., Treu T., Raichoor A., Trinchieri G., 2013, preprint (arXiv:1310.6754)
Nipoti C., Treu T., Bolton A. S., 2008, MNRAS, 390, 349
Nipoti C., Treu T., Auger M. W., Bolton A. S., 2009, ApJ, 706, L86
Papovich C. et al., 2012, ApJ, 750, 93
Peeples M. S., Somerville R. S., 2013, MNRAS, 428, 1766
Poggianti B. M. et al., 2013, ApJ, 762, 77
Posti L., Nipoti C., Stiavelli M., Ciotti L., 2013, preprint (arXiv:1310.2255)
Prugniel P., Simien F., 1997, A&A, 321, 111
Puech M., Hammer F., Hopkins P. F., Athanassoula E., Flores H., Rodrigues M., Wang J. L., Yang Y. B., 2012, ApJ, 753, 128
Ragone-Figueroa C., Granato G. L., 2011, MNRAS, 414, 3690
Raichoor A. et al., 2012, ApJ, 745, 130
Rettura A. et al., 2010, ApJ, 709, 512
Rodríguez-Puebla A., Drory N., Avila-Reese V., 2012, ApJ, 756, 2
Saglia R. P., Bertschinger E., Baggley G., Burstein D., Colless M., Davies R. L., McMahan R. K., Jr, Wegner G., 1997, ApJS, 109, 79
Sérsic J. L., 1963, Bol. Asoc. Argentina Astron. La Plata Argentina, 6, 41
Shankar F., Bernardi M., 2009, MNRAS, 396, L76
Shankar F., Lapi A., Salucci P., De Zotti G., Danese L., 2006, ApJ, 643, 14
Shankar F., Marulli F., Bernardi M., Dai X., Hyde J. B., Sheth R. K., 2010a, MNRAS, 403, 117
Shankar F., Marulli F., Bernardi M., Boylan-Kolchin M., Dai X., Khochfar S., 2010b, MNRAS, 405, 948
Shankar F., Marulli F., Bernardi M., Mei S., Meert A., Vikram V., 2013, MNRAS, 428, 109 (S13)
Shen S., Mo H. J., White S. D. M., Blanton M. R., Kauffmann G., Voges W., Brinkmann J., Csabai I., 2003, MNRAS, 343, 978
Somerville R. S., Primack J. R., Faber S. M., 2001, MNRAS, 320, 504
Somerville R. S. et al., 2008, ApJ, 672, 776
Springel V., 2005, MNRAS, 364, 1105
Stewart K. R., Bullock J. S., Wechsler R. H., Maller A. H., 2009, ApJ, 702, 307
Strazzullo V. et al., 2013, ApJ, 772, 118
Stringer M. J., Shankar F., Novak G. S., Huertas-Company M., Combes F., Moster B. P., 2013, preprint (arXiv:1310.3823)
Taffoni G., Mayer L., Colpi M., Governato F., 2003, MNRAS, 341, 434
Taranu D. S., Dubinski J., Yee H. K. C., 2013, ApJ, 778, 61
Vale A., Ostriker J. P., 2004, MNRAS, 353, 189
Valentinuzzi T. et al., 2010a, ApJ, 712, 226
Valentinuzzi T. et al., 2010b, ApJ, 721, L19
van der Wel A., Bell E. F., van den Bosch F. C., Gallazzi A., Rix H., 2009, ApJ, 698, 1232
van Dokkum P. G. et al., 2010, ApJ, 709, 1018
Vikram V., Wadadekar Y., Kembhavi A. K., Vijayagovindan G. V., 2010, MNRAS, 409, 1379
Watson D. F., Berlind A. A., Zentner A. R., 2012, ApJ, 754, 90
Weinmann S. M., Kauffmann G., van den Bosch F. C., Pasquali A., McIntosh D. H., Mo H., Yang X., Guo Y., 2009, MNRAS, 394, 1213
Wetzel A. R., Tinker J. L., Conroy C., van den Bosch F. C., 2013, MNRAS, 432, 336
Wilman D. J., Fontanot F., De Lucia G., Erwin P., Monaco P., 2013, MNRAS, 433, 2986
Woo J. et al., 2013, MNRAS, 428, 3306
Yang X., Mo H. J., van den Bosch F. C., Pasquali A., Li C., Barden M., 2007, ApJ, 671, 153
Yang X., Mo H. J., van den Bosch F. C., Zhang Y., Han J., 2012, ApJ, 752, 41
Yang X., Mo H. J., van den Bosch F. C., Bonaca A., Li S., Lu Y., Lu Y., Lu Z., 2013, ApJ, 770, 115
Zavala J., Avila-Reese V., Firmani C., Boylan-Kolchin M., 2012, MNRAS, 427, 1503

APPENDIX A: GAS FRACTION IN THE LOCAL UNIVERSE

We discussed in Section 5.1 that models with stronger stripping tend to predict smaller sizes and more pronounced environmental dependence than those without stripping. We here add that these type

Downloaded from http://mnras.oxfordjournals.org/ at INAF Trieste (Osservatorio Astronomico di Trieste) on January 8, 2016

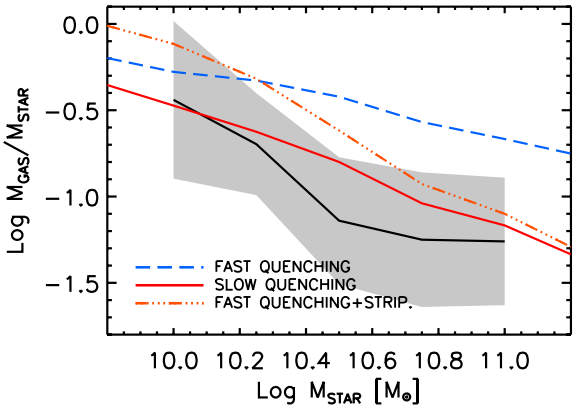

Figure A1. Predicted median gas fraction of bulge-dominated galaxies for the models with continuous star formation in satellites (solid, red) and minimal satellites growth after infall (long dashed, red), compared with the data by Catinella et al. (2010) from the GASS survey for early-type, bulge-dominated galaxies (solid line with grey area marking the 1σ in the full distribution).

of models also produce somewhat different outcomes for the gas fractions in the remnant massive ellipticals. This is clearly evident in Fig. A1, where we compare the resulting gas fractions as a function of stellar mass against the data from the GASS survey by Catinella et al. (2010) for early-type galaxies (solid line with grey area). The model with fast quenching would produce too large gas fractions retained in the remnant galaxies (blue/long-dashed line) compared to the slow quenching one (solid/red line), in which a significant part of the gas in the merging satellites is consumed during infall. Clearly efficient gas stripping must accompany the fast quenching model (orange/triple dot–dashed line) to reconcile model predictions with observations. The latter model is characterized by the same value of $\eta = 0.25$ (equation 13), for both the stars and the gas component, as the stripping model reported in Fig. 2. Overall, a fast quenching+stripping model is quite degenerate with a slow quenching model. However, the former tends to produce too compact remnants at fixed stellar mass and stronger environmental dependence with respect to observations.

APPENDIX B: SATELLITES

So far we focused our attention on central galaxies, as these are the systems for which the effect of mergers is expected to be maximized, being the satellite–satellite merger rate measured to be very low in dark matter simulations (e.g. Angulo et al. 2009). For completeness, this appendix is dedicated to briefly explore and compare the main observed and predicted structural properties of satellites.

Fig. B1 is a collection of three panels. The top, left-hand panel reports the expected size–stellar mass relation from different models, as labelled, for all satellite galaxies with no restriction in the bulge component. We here apply the 3D-to-2D correction only for bulge-dominated galaxies with $B/T > 0.5$, while leave the sizes of disc-dominated galaxies unaltered (e.g. Kravtsov 2013). Both the data and the models show a clear flattening in median size at low masses, below $M_{\rm star} \lesssim 10^{11}\,{\rm M}_\odot$. As evidenced from the two component fitting of SDSS galaxies by Bernardi et al. (2013), the latter feature is naturally explained by the growing contribution of

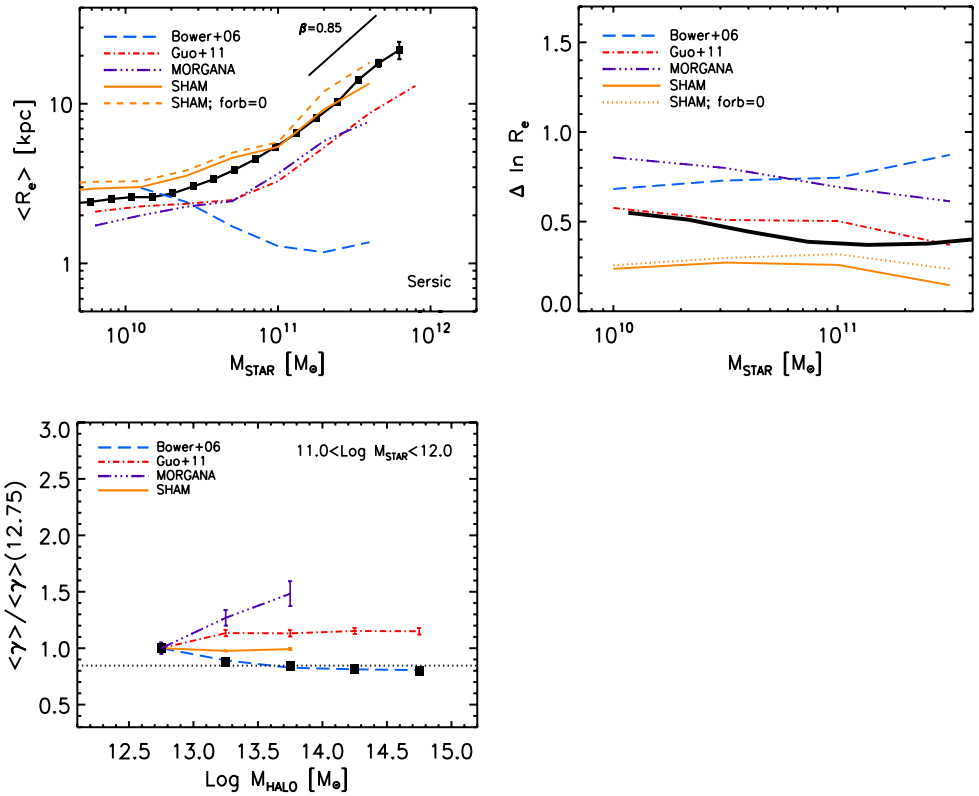

Figure B1. Predicted structural properties of satellites. Top left: size–stellar mass relation in different models, as labelled, compared to data from Huertas-Company et al. (2013b, solid, black line). Top right: predicted scatter around the size–stellar mass relation for the same models and data as in the left-hand panel. Bottom left: median normalized sizes γ, divided by the value at $\log M_{\rm halo} = 12.5$; note that only galaxies with $B/T > 0.5$ have been selected here, to make better contact with the data and previous discussion on central galaxies, but similar results are found even when no cut in B/T is imposed.

Downloaded from http://mnras.oxfordjournals.org/ at INAF Trieste (Osservatorio Astronomico di Trieste) on January 8, 2016

discs progressively dominating the structural properties of galaxies at lower stellar masses. What is most relevant here is that, except for the B06 model, all models share size distributions for satellites in broad agreement with those observed. In other words, the satellites, which eventually will merge with their centrals, have the correct sizes.

The upper right-hand panel plots the scatter around the median relation for the same models compared with the data (solid line). As for centrals, models tend to predict larger distributions, although the difference is limited for the G11 model and absent for the SHAM model, both characterized by low disc instabilities and, at least the latter, by tight correlations for the infalling satellites (see Section 5.2).

The lower-left panel shows that the environmental dependence of satellites is overall quite limited by up to 20–30 per cent. Here only raw model predictions are reported, the convolution with (correlated) errors will clearly cancel these relatively modest trends with environment. Overall, satellites tend to present somewhat less environmental dependence with respect to centrals of similar stellar mass (Fig. 7). Particularly striking is the difference from centrals to satellites in the B06 model, for which the dependence is actually reversed. Satellites are a mixture of galaxies with different morphologies and accretion histories. Their varied evolutionary histories bring them to live in very disparate environments, much more than their counterpart centrals of similar stellar mass, thus decreasing any environmental signal (see also Huertas-Company et al. 2013b).

This paper has been typeset from a TEX/LATEX file prepared by the author.

Downloaded from http://mnras.oxfordjournals.org/ at INAF Trieste (Osservatorio Astronomico di Trieste) on January 8, 2016